Analysis of the influence of a lake on the lower convective boundary layer from airborne observations

Andreas Platis [1], Daniel Martínez Villagrasa [2,1], Frank Beyrich [3] and Jens Bange [1]

[1]Zentrum für Angewandte Geowissenschaften, Universität Tübingen
[2]University of the Balearic Islands, Palma, Mallorca, Spain
[3]Deutscher Wetterdienst (DWD) Meteorologisches Observatorium Lindenberg

August 30, 2016

Abstract

The influence of an intermediate-scale lake, with a dimension of approximately 2 km $\times$10 km, on a convective boundary layer has been analysed. Data were collected by the airborne platform Helipod during the STINHO 2002 and LITFASS 2003 campaigns in eastern Germany, during early summer months, when the lake was much colder than the surrounding surface. The objective was to assess which atmospheric parameters show influence from the lake by the airborne observations. While spatial variability for mean quantities is not significant at the observation height of 70 m and above, the second-order statistics related to potential temperature exhibit a clear decrease in the vicinity of the lake for measurements taken below 100 m above ground level. Second-order statistics of humidity and vertical wind velocity are not suited to identify the foot print of the lake in our study. Several length scales of surface heterogeneity were calculated following previous studies. Only the scale that considers vertical velocity is compatible with our airborne observations. In addition, the application of a convective scale indicates that the lake could affect the lower convective boundary layer above the lake and above the surrounding land downstream of the flow for low wind speeds (below 4 m s^{-1}). Finally, the downstream propagation of the lake influence has been addressed by calculating the cross-correlation function between the surface radiative temperature and the variance of potential temperature. A clear relationship between the spatial lag of the maximum correlation and the horizontal advectivon could be identified.

Keywords: Helipod, Lake, LITFASS 2003, Convective boundary layer, Surface heterogeneity influences, second-order statistics, turbulence

1 Introduction

Local and regional climate and weather is affected by the interaction between the land and the atmospheric boundary layer (ABL) and depends highly on the surface characteristics, which may influence the spatial structure of the ABL. Natural landscapes are usually heterogeneous with different surface types like patches of farmland, water, villages, forests, etc., each with different heat, moisture and roughness characteristics. These specific features accompanied with different scales of surface heterogeneity (usually varying from meters to kilometers), generates different sizes and strengths of turbulent eddies which affect the overlying convective boundary layer (CBL). Therefore, the vertical extension of this influence depends on the characteristic horizontal scale of surface heterogeneity (L_{het}), the turbulence intensity, thermal stability and the horizontal advection of the boundary-layer flow (Mahrt, 1996). The horizontal variability of the turbulent structure may be influenced by both the length scale and amplitude of the surface heterogeneity (Mahrt, 2000).

A number of studies addressed the interaction between a heterogeneous surface and the ABL mostly by high-resolution large eddy simulation (LES) in the last 25 years (Hadfield et al, 1991, 1992; Avissar and Schmidt, 1998; Letzel and Raasch, 2003). They have found that the simulated CBL structure was strongly affected by the spatial variation of surface heat flux and that larger scales of landscape heterogeneity have more influence on the CBL. However, many studies have been performed with simplified surface conditions and only one dimensional heterogeneous heat flux fields.

Simulations with realistic surface data from field campaigns have been performed only recently as they demand high computational resources (Sühring and Raasch, 2013; Maronga and Raasch, 2013; Maronga et al, 2014; Huang and Margulis, 2009). Based on the LES results from two selected cases of the Lindenberg Inhomogeneous Terrain - Fluxes between Atmosphere and Surface: A long-term Study (LITFASS 2003) campaign with ground-based measured surface forcing data as an input for LES, Sühring and Raasch (2013) and Maronga and Raasch (2013) concluded that the influence of surface heterogeneity is present throughout the entire boundary layer for both sensible and latent heat fluxes during strong CBL conditions. They did not detect any blending height (above which the influence of the surface heterogeneity vanishes) for convective conditions and L_{het} larger than the boundary layer height z_i. In another LITFASS-2003 case study Maronga et al (2014) showed by LES that local effects of surface heterogeneity remain prominent in the lower ABL. They could not give any proof for a blending height for the temperature structure parameter (a measure for temperature fluctuation similar to the temperature variance σ_θ), but for the LITFASS-2003 case study it seems that blending of the temperature structure parameter occur above several tens of metres above the ground. Furthermore, they conclude that the structure parameter for temperature is highly correlated with the surface sensible heat flux. However, structure parameter for humidity (describes the strength of humidity fluctuations) is decoupled from the latent surface flux even at low levels which is ascribed to the entrainment of dry air at the top of the boundary layer. Huang and Margulis (2009) discovered that potential temperature is more sensitive to surface heterogeneity than humidity. By using vertical profiles of temperature variance they could identify a thermal blending height in a CBL which was in good agreement to predictions from Wood and Mason (1991) and Mahrt (2000).

The blending height is viewed here as a scaling depth that describes the decrease of the influence of surface heterogeneity with height. A blending height is not a sharp boundary where the influence of surface heterogeneity suddenly and completely vanishes, but it describes a vertical scale at which the impact of surface heterogeneity decreases to some relatively small value. Different formulations of this height have been discussed in the literature, depending on which forcings are more relevant (for a complete review see Mahrt, 2000; Bange et al, 2006). The blending height can be re-formulated in terms of internal boundary layers (IBL). An IBL grows to a maximum depth which is small compared to the upstream boundary-layer depth, and then encounters a new surface type and looses surface support (Mahrt, 2000). An IBL is expected if a clear change in the mean variables is identified.

Flow of marine air over a heated land surface is a classic example of the mesoscale internal boundary layer, see references in Garratt (1990). Another possible location where an IBL can form is above a lake. Unlike a large uniform open ocean the fetch above a lake is typically limited, which supports the development of a local IBL. Panofsky et al (1982) and Højstrup (1982) already demonstrated that the variance spectra of the horizontal wind components in an IBL were influenced by upstream conditions. However, on smaller scales like an intermediate-size lake (only a few kilometres width) a well defined surface discontinuity is not necessarily transferred into the flow since the boundary layer may adjust without the formation of a new IBL. This situation may be enhanced when the change of surface properties is not sharp or is of small amplitude (Mahrt, 2000). An adjusting boundary flow is characterized by horizontal changes of some of the higher moments but does not exhibit significant horizontal variation of the mean variables. Such boundary-layer adjustments are probably common for smaller surface heterogeneity scales, like the intermediate-sized lake in our study, but have received little attention so far.

Comprehensive studies of the direct influence of a lake on the lower ABL are scarce. Sahlée et al (2014) showed that the structure of the turbulence above the lake is influenced by the surroundings. Variance spectra of both horizontal velocity and scalars during both unstable and stable stratification displayed a low frequency peak. However, a lack of concurrent observations over the adjacent land, precluded any comparison of the spatial structure between land and lake. In a study from Samuelsson et al (2010) the impact of lakes on the European climate was considered. A simulation where all lakes in the model domain are replaced by land surface is compared with a simulation including lakes. The numerical results stated that the lakes induce a warming on the European climate for all seasons. However the study does not show any direct impact on the boundary layer or the local flow. Based on airborne observations obtained during the Upper Spencer Gulf experiments in South Australia, Shao et al (1991) and Shao and Hacker (1990) investigated the structure of turbulence in a coastal boundary layer, which is an extreme case of horizontal inhomogeneity. They showed that the boundary layer over this highly non-uniform surface is characterized by extensive variations in its thermal stratification and turbulence characteristics and that the behaviour of statistical parameters of second- and higher moments seemed to be determined mainly by local forcing. Bange et al (2006) analysed airborne measurements from the LITFASS-2003 and Structure of the Turbulent transport over INHOmogeneous surfaces (STINHO-2) field campaigns to study the response of second-order statistics like turbulent flux profiles to a patchy landscape with different underlying surfaces like farmland, forest and a lake. The case studies showed that the sensible heat fluxes determined over the different sub-areas presented clearly different values at surface level and at 80 m. Especially, the vertical profiles over water surfaces produced its own vertical profile of sensible heat flux under weak-wind conditions, apparently unaffected by the surrounding forest and farmland.

Aforementioned works like Sühring and Raasch (2013) and Bange et al (2006) show evidence that the lake has an influence on the vertical profile of latent and sensible heat fluxes above the lake. However, the authors did not find any scaling depth (as those by Mahrt, 2000; Strunin et al, 2004) that could successfully predict the conditions for a horizontal mixing state of the CBL. In addition, none of the scaling parameters analysed by e.g. Bange et al (2006) and Sühring and Raasch (2013) were successful in predicting the vertical extension of the surface heterogeneity or explaining the spatial variability of latent heat fluxes. One possible explanation could be that too many different types of surfaces, and hence heterogeneity scales, where involved in such analysis. Further Sühring and Raasch (2013) argued that those flights in Bange et al (2006) that showed horizontal mixing had a poor statistical representation of the mean flux estimation from a single leg and thus, they are not suitable for such studies.

In the present study airborne measurements from LITFASS-2003 and STINHO-2 field campaigns (Beyrich et al, 2002; Beyrich and Mengelkamp, 2006) are analysed in order to evaluate if the influence of a lake on spatial structure of the convective boundary layer (CBL) is apparent. The lake is of intermediate size with a dimension of approximately 2×10 km^2 and called Scharmützelsee. It represents a surface heterogeneity with a well defined length scale (lake boundaries) and a sharp and strong change in surface conditions. This is because it has a colder and smoother surface and is surrounded by warmer and rougher terrain during the measurement period in late spring and early summer time. Additional flights from the field campaigns used in Bange et al (2006) and Sühring and Raasch (2013) were analysed. We report comprehensive observations of the lake influence on the first and second order statistics like the variance of temperature and humidity by airborne measurements and depict the limitations of such measurements regarding the statistical significance. We determine the key parameters that contribute to the observed spatial changes over lake and land and show as well the lack of lake influence on certain parameters. Further, we try to characterize the horizontal shift of the lake influence. The study evaluates if an IBL can be observed for the LITFASS-2003 area and describes in more detail the downstream propagation of the lake-influenced boundary layer. We follow the suggestions and analysis of blending heights and IBL published by Raupach and Finnigan (1995); Mahrt (1996, 2000); Wood and Mason (1991). The proposed minimum horizontal scale (L_{het} which is described by theses studies) of the surface heterogeneity that would influence the airborne measurements at observation level, is checked and compared with the current airborne data set.

Section 2 briefly describes the experimental dataset used in the present study. The main flow characteristics close to the surface over the lake-land discontinuity as well as an error discussion are addressed for a case study in Sect. 3, with an extension to the rest of selected cases. Section 4 assesses the length scales that describe the vertical extension of surface heterogeneity with the current dataset, while Sect. 5 studies the stream wise propagation of the heterogeneity influence. Finally, a conclusion is presented in Sect. 6.

2 Experiment

2.1 Dataset

The data analysed in this study were collected during two consecutive field campaigns in the summers of 2002 and 2003, that were part of the series of the LITFASS experiments. This program was initiated in 1995 in order to develop and test a strategy for the determination of the area-averaged turbulent fluxes over a heterogeneous landscape (see Beyrich et al (2002) for more details). The STINHO-2 experiment took place between 24 June and 10 July, 2002, (Raabe et al, 2005), while the LITFASS-2003 campaign was carried out between 19 May and 17 June, 2003 (Beyrich and Mengelkamp, 2006).

Both campaigns were performed around the MOL-RAO (Meteorological Observatory Lindenberg - Richard-Aßmann Observatory) of the German Meteorological Service (Deutscher Wetterdienst, DWD) in the area of Brandenburg, Germany, 60 km south-east from Berlin. The experimental site is a 20 $\times$ 20 km^2 flat area with an elevation difference across the site of less than 100 m. The region consists of a coniferous forest in the western part (43% of the area) and agricultural fields in the eastern part (31%, mainly cereals). The whole area is covered by lakes and villages that add heterogeneity to the field. The lake Scharmützelsee has a dimension of approximately 2×10 km^2, and the long-axis is mainly oriented north-south.

The campaigns were part of the EVA_GRIPS (regional EVAporation at GRId/Pixel Scale over heterogeneous surfaces) and the VERTIKO (VERTIcal transport of energy and trace gases at anchor stations under Complex natural conditions) networks and provided a comprehensive data set on surface-atmosphere interaction processes at the mesoscale (Mengelkamp et al, 2006; Göckede et al, 2004). Measurements included the instrumentation equipment from the Falkenberg boundary-layer field site (GM Falkenberg) of DWD, a regional network of micro-meteorological stations, the 99-m meteorological tower and airborne measurements sampled by the helicopter-borne turbulence probe Helipod, among other ground-based remote sensing devices (see Raabe et al (2005) and Beyrich and Mengelkamp (2006) for a complete overview).

The Helipod is a measurement system designed for boundary-layer field experiments. It is an autonomously operating sensor package attached to a 15 m rope below a helicopter of almost any type. The Helipod is equipped with its own power supply, on-board computer, data storage, navigation systems, radar altimeter and carries a sensor equipment for in-situ measurements of the atmospheric wind vector, humidity and air and surface temperatures at 100 Hz sampling rate. The resolution of the fast resistance temperature sensor is high (much better than 0.1 Kelvin) and about 30 Hz, which is fast enough to resolve turbulent temperature fluctuations (Bange and Roth, 1999). Hence, it is suited for small-scale turbulence measurements and for calculating the turbulent fluxes using the eddy covariance method. The surface temperature is measured by an infrared temperature sensor simultaneously with the thermodynamic measurements. At a mission speed of 40 m s^{-1} the Helipod is outside the down-wash area of the helicopter's rotor blades. More details can be found in Bange et al (2002) and Bange and Roth (1999).

More than 100 flight hours of Helipod data were compiled during these two field campaigns. A total of 14 flights that covered the lake-land transition were selected, 13 from the LITFASS-2003 experiment and an additional one from the STINHO-2 experiment (see Table 1). Basically, all flights included in this study had at least one leg crossing the lake in a west-east direction at about 100 m above ground level. In the following study all given heights are always with respect to the ground level.

All selected flights that contribute to our particular database were performed either in the morning or in the early afternoon in a convective regime, although with different wind conditions. Three types of flight patterns can be recognized from this data base, that will be referred as 'IBL-lake', 'North Box' and 'E-W grids' for the rest of the text (Fig. 1a and 1b and Table 1). There are three flights that crossed the lake approximately parallel to the mean wind direction during the flight (IBL-lake, see Fig. 1a), which was either southeasterly (STI09) or northwesterly (LIT13, LIT14). The rest of them contain legs in the west-east direction, crossing the lake at different heights over the same latitude (North Box) or over three different sections of the lake, from the southern edge to the middle part of the lake (E-W grids), see Fig. 1b.

2.2 Data analysis

We have analysed the spatial series and the second-order statistics for potential temperature θ, water vapor mixing ratio m and wind vector components. In order to study how the surface heterogeneity affects them and up to which height, it is necessary to determine a suitable horizontal length scale over which we compute the first- and second-order statistics within sub-legs (data windows) along a flight leg. As an example, the potential temperature variance is computed as

$$\sigma_\theta^2 = \frac{1}{N}\sum_{n=1}^{N}(\theta_n - \overline{\theta})^2 \qquad (1)$$

where N is the number of data points within the moving data window. The width of this window has to be small enough to resolve the surface heterogeneity along the leg, but large enough to cover the main scales that contribute to the turbulent fluctuations. van den Kroonenberg et al (2012) defined (for a similar experiment at the same site) a minimum window width of twice the integral length scale to ensure that all turbulent scales within the inertial sub-range are included. Previous studies of our dataset show that the integral length scales of sensible and latent heat fluxes measured by the Helipod are smaller than 500 m (Bange et al, 2006). Thus, we have defined windows of 1-km width using unweighted means, sequentially shifted through the leg by increments of 250 m. In summary, for flux calculations, this value does not necessarily account for the largest eddies during strong convection conditions. However, 1-km width is a good compromise between the largest eddy scales within the surface layer and the detection of a possible lake influence. A similar strategy was followed by Mahrt (2000). For all these reasons, we believe that 1-km window is expected to capture almost all of the turbulent flux and its spatial variability. A more precise discussion on the sampling error is given in Sect. 3.2.

3 Results

3.1 STINHO-2 Flight (STI09)

The flights chosen for the analysis of the land-water transition around lake Scharmützelsee (Table 1) were composed by straight and leveled paths (called legs) at different heights, ranging from 70 to 280 m. The distance of each single leg was between 7 and 16 km and covered different surface patches (forest, farmland, lake) along the leg. The main interest of this study is the impact of the lake. The influence of other patches, which are not in the vicinity of the lake, are not important. Those which are located close to the lake may influence the signal as well. However, the impact is very low since length scales of the other patches are much smaller than the lake width. Further, surface discontinuities, i.e. the change in surface forcing for the other patches is much lower than between land and water.

In order to study the influence of a surface discontinuity, it is appropriate to have a fine grid of legs closer to the surface. While all selected flights contain at least one leg below 100 m, only the STINHO-2 flight includes several legs within the first 100 m above ground. Therefore, this particular flight has been chosen for the initial study of the lake-land discontinuity influence on the CBL.

The flight performed on the 9th June 2002 (STI09) was composed of five legs crossing the lake over its middle part and are called middle track (MT) hereafter as shown in Fig. 1a. These legs were performed between 40 to 280 m, following a direction approximately parallel to the mean wind. The sky was only slightly cloudy (2/8 Ci), with a mean wind speed of 6 m s^{-1} from south-east direction (150°) at 100 m height. Table 2 shows the chronology of the legs of this flight. On that day, the CBL height z_i reached a value of 2100–2300 m, as derived from the wind profiler data (Beyrich and Mengelkamp, 2006).

Figure 2 shows the altitude variation along the five legs flown over the middle part of the lake. All legs contain significant changes in altitude, because the Helipod did not maintain a constant height above ground level. Since the three lowest legs overlap partially within a layer between 40 and 120 m, they will be analysed together to describe the flow characteristics close to the surface (0.02 z_i–0.05 z_i). The complete flight lasted more than one and a half hours in the early afternoon. Within this period, the air temperature increased approximately 1 K, mainly due to the diurnal cycle. This warming trend was also observed in data from the 99-m tower at the Falkenberg site (not shown). During these flights, moisture and wind vector for the mean flow did not show significant changes. This warming effect must be considered in the attempt to use the three legs performed below 100 m as different iterative measurements of the same layer. Further, we can assume that the CBL and the second-order statistical moments remain stationary. Indeed, during the 1.5 hour STI09 flight the radio sonde observations (not shown) show that the CBL grew from 1825 m (1052 UTC) to 2375 m (1637 UTC). Assuming a linear trend, that gives an evolution of 100 m hour^{-1} (150 m of growth for the entire flight). This change in the boundary-layer height can be ignored. Regarding the second-order moments, the surface fluxes close to the surface did not changing significantly during the flight time (Beyrich et al, 2006). Even if fluxes would change, we are only interested in the local differences of fluxes that are simultaneous. That is, the relation of local fluxes respect to their spatial averages for a given time. In this sense, the overall time evolution is not important.

3.2 Sampling Error

The second-order statistics like the standard deviation measurement itself are subject to errors. Flight legs that are not large enough compared to the largest energy-transporting eddies cause a systematic error since they lead to a systematic under- or overestimation of the turbulent flux or standard deviation (Grossmann et al, 1994). The sampling error can be estimated by the expression stated by Mann and Lenschow (1994) and Lenschow et al (1994) representing the absolute systematic statistical uncertainty of the standard deviation σ_θ related to a single flight leg on which σ_θ was calculated:

$$\Delta\sigma_\theta = 2\frac{I_\theta}{P_l}\cdot\sigma_\theta \tag{2}$$

where I_θ is the integral length scale (see van den Kroonenberg et al, 2012) of θ and P_l the averaging length. Since I_θ is about 500 m during our flights and P_l about 1000 m (see Sect. 2.2), the sampling error becomes

$$\Delta\sigma_\theta \approx \sigma_\theta. \tag{3}$$

Furthermore, different measurements of finite duration or length under identical boundary conditions lead to different second-order statistics compared to the ensemble mean (Bange et al, 2013). Over land the standard deviation changes significantly over different passes as a consequence of turbulent elements. This is expressed by the random error. For σ_θ the random error $\sigma^2_{\sigma_\theta}$ is defined as the averaged squared differences between the ensemble and the actually measured standard deviation. Thus, σ_{σ_θ} can be interpreted as the standard deviation of σ_θ. An estimate is given by Lumley and Panofsky (1964); Lenschow and Stankov (1986) and is defined by:

$$\sigma^2_{\sigma_\theta} = 2\frac{I_{\sigma_\theta}}{P_l}\cdot\overline{(\sigma^2_\theta)'^2} \tag{4}$$

with

$$\overline{(\sigma^2_\theta)'^2} = \frac{1}{I-1}\sum_{i=1}^{I}(\sigma^2_\theta(i) - \sigma^2_\theta(\text{leg}))^2 \tag{5}$$

where I is the number of (moving) data windows on one single flight leg. For instance on a 15 km long leg, $I = 15,000/250 = 60$ values for the variance (in Eq. 1) are calculated. $\sigma_\theta(\text{leg})$ is the spatial average of the standard deviation of θ along the whole flight leg:

$$\sigma_\theta(\text{leg}) = \frac{1}{I}\sum_{i=1}^{I}\sigma_{\theta_i} \tag{6}$$

The total error of the measurement is the sum of σ_{σ_θ} and $\Delta\sigma_\theta$. Therefore, the uncertainty is in the same order of magnitude as σ_θ itself. The same also applies for the water vapor mixing ratio m. Generally, this influence can be reduced by averaging over all the passes for a given flight for each window. Unfortunately, this technique requires the performance of iterative passes along the same leg. In our dataset, the flights from the LITFASS-2003 campaign do not include more than one pass per leg, precluding the application of this technique. Only the selected STI09 flight includes three passes along the lowest leg. However, also the information of the LITFASS-2003 flights is qualitatively valuable and useful, especially when all flights are treated together as done in Sect. 3.5.

In Fig. 3, σ_θ of the three lowest passes (MT02, MT12, MT16) of STI09 flight are shown. The average $\overline{\sigma_\theta}(i)$ over the number of passes P (in our case $P = 3$) is marked by the red line and its error bars for each (moving) window i along the flight leg. The error bars ζ_{σ_θ} are calculated by the statistical square average of the variation between σ_θ and $\overline{\sigma_\theta}$ for each (moving) window i along the flight leg:

$$\zeta^2_{\sigma_\theta}(i) = \frac{1}{P-1}\sum_{p=1}^{P}(\sigma_\theta(p,i) - \overline{\sigma_\theta}(i))^2 \tag{7}$$

The uncertainty ζ_{σ_θ} derived from measurements over the lake is significantly smaller than the observed drop in σ_θ over the lake, indicating that this drop is most likely related to the lake footprint. However, the following analysis has to be considered with caution. Even though the error is too high for a quantitative analysis, yet the lake remains qualitatively recognizable. A similar result is obtained for the standard deviation of the water vapor mixing ratio σ_m or the latent and sensible turbulent heat fluxes.

3.3 First-Order Statistics

Figure 4 shows the window average of potential temperature along the legs performed over the middle part of the lake. The warming trend of 1 K observed during the flight has been removed from the lowest three legs for better comparison. The window-averaged surface temperature, as measured from the lowest leg, has been also included. This variable reflects the presence of the lake, which is 15 K cooler than the surrounding area. Over land, lower surface temperatures allow the forest cover to be distinguished from farmland at both sides of the lake.

Considering the three lowest legs below 100 m, there are large variations of potential temperature over land. However, a cooling effect of approximately 0.5 K is observed over the lake, which is shifted downstream to the west between $X = 5$ - 6 km, since the prevailing wind direction is from the south-east. Note, that X is defined as the distance from an arbitrary point at the western edge of the flight paths. The standard deviation of potential temperature also decreases significantly over this part of the leg, as we will discuss later. This cooling effect related to the lake is hardly detected at 170 and 280 m (MT04 and MT06, respectively).

The average water vapor mixing ratio m (Fig. 5) presents some variability along the legs that does not allow for clear detection of any lake influence. Over the forests at $X = 4$-5 km and 13-15 km a weak maximum of m is detected. Since the lake is partially surrounded by trees, with the large forest at the south of the lake, it is therefore possible to distinguish a drier atmosphere over the lake compared to the moister air over forest. The upper legs do not exhibit similar patterns. Strong convection plays a role on the variability of θ and m for the different passes as described in Mahrt (2000). However, the spatial organization and variability for both variables are not similar, indicating that m may be affected by other factors, e.g. such as entrainment, which is not directly related with surface patterns (Sühring and Raasch, 2013). Bange et al (2006) and Sühring and Raasch (2013) noted that the latent heat flux is more affected by the entrainment of dry air from the free atmosphere than by the surface latent heat flux during LITFASS-2003 experiment, in contrast to the temperature, which is more affected by the sensible heat flux.

3.4 Second-Order Statistics

The smaller variability of the potential temperature over the area of the lake influence is further analysed in Fig. 6, where the standard deviation of potential temperature σ_θ is represented along the MT legs. As indicated in Sect. 3.3, a clear drop in σ_θ is present for the three lowest legs, shifted westward of the lake, following the mean wind direction. Such a horizontal displacement can be an indication for the lake footprint propagation downstream.

At the upper levels, the lack of multiple passes complicates the interpretation of σ_θ with respect to the lake influence. This analysis has to be consider as speculative. At 170 m (MT04), the leg segment with small variances over the lake is extended downstream ($X = 3$-6 km), while it is much narrower and closer to the lake at 280 m (MT06) between $X = 5$-6 km. However, σ_θ exhibits lower values also over other regions of theses legs (i.e. the farmland/forest area between km 11 and 14 at leg MT04) or upstream the lake at MT06), leading to an unconfined statistical significance..

The standard deviation of water vapor mixing ratio changes significantly over the different passes at lower heights, including those segments over the lake (Fig. 7). These results seem to indicate a rapid change of σ_m over the lake, specially compared to the surrounding area closer to the lake's shorelines. However, no statistically significant minimum is observed over the lake. Sometimes the spatial change of the instantaneous m can be very large across the forest-lake discontinuity, especially with the fact of a comparable large window size of 1 km, producing a sudden peak on σ_m (Fig. 5). This is the case for the large value detected over the western shoreline in MT12. For the rest of legs, the value of σ_m does not indicate the presence of the lake.

The variance of vertical velocity σ_w for the MT legs increases for higher altitudes (Fig. 8) corresponding to CBL theory. At the lowest heights, it does not show any terrain influence. At higher levels, however, its variability increases as the leg-average value also increases. At 280 m, σ_w is smaller at the eastern and western shoreline of the lake.

Another important scaling variable is the surface Reynolds' stress, when turbulence is modulated by wind shear near the ground. This stress is expressed by the vertical flux of horizontal momentum known as the friction velocity u_*, defined according to Stull (1988) as

$$u_* = \left[\overline{u'w'}^2 + \overline{v'w'}^2\right]^{1/4} \tag{8}$$

The leg-averaged friction velocity u_* does not vary significantly with height for the MT legs (Figure 8), indicating that the variance of vertical wind increases with height due to convection. However, the spatial distribution of u_*, and σ_w is very similar along the legs, showing that they are related, following the decomposition from the model of σ_w in Højstrup (1982). Similarly, closer to the surface u_* does not exhibit a clear relationship with the surface pattern.

Since the variance of the vertical wind below 100 m does not reflect any surface influence for MT, the behaviour of the sensible and latent heat fluxes (Fig. 9) are very similar to those described for potential temperature and water vapor mixing ratio. Due to a stable stratification over the cold water during the day and its effect on suppressing turbulence (Beyrich et al, 2006), the sensible heat flux presents small or even negative values over the lake along the MT legs for the lowest levels, indicating a negligible or downward heat flux. Higher legs do not show any influence of the lake (not shown).

Similar to σ_m, the spatial distribution of the latent heat flux (Fig. 9) changes significantly for the different passes over the lake, precluding the detection of any lake influence in our dataset. Even for the latitudinal north-south legs, performed exclusively over the lake, the latent heat flux presents significant differences (not shown), indicating that the latent heat flux in the surface layer responds to dynamics originating from a larger scale.

3.5 Flights LIT13 and LIT14 (2003) and discussion with STI09 (2002)

In the following, two additional flights (performed during the LITFASS-2003 campaign) are analysed, that were carried out on a flight pattern similar to the STI09 flight (in 2002), see Fig. 1a. The LITFASS-2003 campaign took place in June 2003, when the weather was characterized by high insolation and temperatures were mostly above 10 ^{o}C at night. However, several rain events modified the day-to-day weather characteristics, providing cases with a large variety of wind and buoyant conditions. They included several straight legs that crossed the lake over the same region as the MT legs described in the previous sections. The flights consisted of five legs at different levels approximately parallel to the mean wind direction which was the Northwest in both cases. LIT13 was performed in the early afternoon of a mostly sunny day but with 5/8 of Cirrus clouds. A storm event took place during the previous morning and early night, leaving a wet land surface with a mean wind speed of 8 m s^{-1}. On the next day, LIT14 was performed in the morning, with the sky partially covered with cirrus and convective clouds and a mean wind speed of 4 m s^{-1}. The effect of the surface humidity was identified on the leg-averaged sensible heat flux at 90 m, with smaller values for LIT13 (110 W m^{-2}) than LIT14 (160 W m^{-2}). Despite of the different surface conditions for both flights, a decrease in both potential temperature mean and variance can be identified over the lake for the lowest leg (Fig. 10). Although there is less statistical significance by the flights with a single pass, most of them show a drop σ_θ at the vicinity of the lake. This is not significant if each flight is taken individually, but its persistence for most of the flights is a useful information.

A clear lake influence on the rest of the variables is difficult to identify since there is only one pass for each level.

In summary, the data analysed for the three flights (STI09, LIT13 and LIT14) indicate similar results, although the lack of several passes per flight along the same path exclude a definitive statement of lake influence. The lake produces a small cooling effect over the first 100 m, which is shifted progressively downstream. However, the decrease of θ is only a few tenths of Kelvin around 80 m. The variance of potential temperature is clearly affected by the presence of the lake by showing a drop of σ_θ (Fig. 6 and 10), despite of the mean wind and buoyancy conditions. The variance of m is not so clearly affected by the lake. A decrease is indicated over the lake, but sometimes, the spatial change of the instantaneous m is large across the forest-lake discontinuity, producing a sudden peak on σ_m.

The presence of the lake does not affect the strength of turbulent mixing in the surface layer (either represented by σ_w or u_*, see Fig. 8) at observation height. However, the sensible heat flux is very small or even negative over the lake as shown by the small variance of potential temperature. Latent heat flux behaves differently. Moisture distribution responds with a more complex pattern to the surface forcing (due to the presence of forest, agricultural fields and urban areas), and thus the variance of m can be equally large over the lake as over other regions. In general, θ and σ_θ show the strongest and most significant footprint of the lake, with a decrease of values, although this is consistently visible at the lowest flight level of about 80 m only. The results indicate that predictions by LES in former literature e.g Maronga et al (2014) or Huang and Margulis (2009), where temperature variance is more sensitive to surface heterogeneity than humidity is observed as well in the in-situ data.

3.6 Lake influence on the rest of flights

An analysis of the rest of LITFASS-2003 campaign flights reveals a similar behaviour in σ_θ. A total of 34 legs crossing over the lake, within the first 100 m, have been analysed. The main difference, with respect to the flights described above (LIT13, LIT14, STI09), which followed the mean wind direction, is that these legs were always oriented in west-east direction, (Fig. 1b). Flights LIT24, LIT25 and LIT07 applied a vertical matrix at three levels for different days, all characterized by a mean wind direction from the SE but by different speeds. Additionally eight flights were analysed, each one contributing with three legs below 100 m. These flights were performed under different ambient conditions, regarding the mean wind direction, time of the day (either morning or early afternoon) and cloud cover.

In order to detect a systematic influence of the lake on the measurements at the lowest levels, a search for drops in σ_θ has been applied to all LITFASS-2003 flights (including LIT13 and LIT14). For this purpose, it is necessary to define the following parameters as shown in the schematic in Fig. 11:

- Leg-average $\sigma_\theta(\text{leg})$: It represents the mean of the σ_θ obtained for each window i of 1 km width sequentially marched through the leg by increments of 250 m, see Eq. 6.
- Local-average $\sigma_\theta(A)$: defined as the mean value of σ_θ for three consecutive 1-km windows. This parameter is only evaluated for those 1-km windows that fall within a horizontal distance of ± 2 km from the lake boundaries. This restriction in the horizontal distance was applied for preventing those drops in σ_θ whose physical relation with the lake is unlikely in order to avoid other elements that may add mor noise to the data. The STI09 Flights give us a reasonable justification to relate any significant drop of σ_θ at the vivinity of the lake with the presence of the lake. The value of the threshold (± 2 km) was determined after a qualitative revision of the σ_θ evolution for all flights.
- The centre of the segment with the lowest $\sigma_\theta(A)$ or, similarly, with the largest value of $\sigma_\theta(\text{leg}) - \sigma_\theta(A)$ is identified as the central point of the region with the largest influence of the lake, which is assumed to have the same width as the lake. Additionally, the horizontal distance between this point and the centre of the lake is defined as the observed mean propagation distance of the lake influence δx_{obs}, at the leg height $\bar{z}_{\text{obs}}$. This horizontal distance will be used in Sect. 5.

A clear drop in σ_θ was detected by the computer algorithm search over the lake for all legs except for one case. An example for the flight LIT13 and LIT14 is shown in Fig. 10. Circles there mark the segment of the leg where the drop of σ_θ is maximum in the vicinity of the lake. It should be noted that other drops occur as well along the flight leg, as seen for example at X=22 km for LIT14 in Fig. 10. In that case this is probably the influence by another lake. However, the programmed algorithm detects only drops in the vicinity of the lake Scharmützelsee. Moreover the decrease in magnitude of this drop exceeds 50% of the leg-averaged σ_θ for 29 cases. Considering that these results are based on single passes along the given legs, where the random error can play an important role in the determination of the turbulent variances, the drops are significant and confirms previous results in Sect. 3.5.

4 Vertical propagation of the lake influence

The blending-height theory addresses the decreasing influence of surface heterogeneity with height, identifying a scaling depth where this influence progressively vanishes. Different formulations of the blending height z_{blend} have been discussed in the literature (Mahrt, 2000; Raupach and Finnigan, 1995; Wood and Mason, 1991), depending on which forcing is most relevant. The different blending height formulations are compared and checked with our in-situ data in order to estimate which formulation is the most relevant for our data set. Since 33 out of 34 legs showed an influence of the lake on the measurements of the standard deviation of potential temperature at 100 m, we should find a parametrization which fits to almost all of our cases, indicating a scaling depth larger than our aircraft observation height. All formulations are proportional to the length scale of the surface heterogeneity L_{het}, a stability parameter ψ, which is a measure of the stratification or wind shear production of turbulence, and they are inversely proportional to the wind speed $\overline{u}$ (Mahrt, 2000),

$$z_{\mathrm{blend}} = C_\psi \left(\frac{\psi}{\overline{u}}\right)^p L_{\mathrm{het}} \tag{9}$$

where C_ψ and p are non-dimensional coefficients that take a particular value for each formulation. The stability parameter and wind speed are leg averaged. That means each parameter is first calculated within each 1 km window sequentially shifted through the leg by increments of 250 m. Second, all 1 km window parameters of each flight leg (around 54 for a 14 km long flight leg) are then averaged. In this sense, we attempt to receive a parameter which is representative of the whole heterogeneous area. When turbulence is shear-generated, local diffusive mixing dominates and the stability parameter ψ becomes the friction velocity u_*, with $p = 2$ and C_ψ is in the order of 1. With $p = 1$, we obtain the diffusion height z_{diff} (Wood and Mason, 1991), a level at which effects of the surface heterogeneity completely vanish.

When surface heating is important, Wood and Mason (1991) suggested using the spatially-averaged surface heat flux and potential temperature, $\psi = \left(\overline{w'\theta'}\right)_0 / \overline{\theta}_0$, to explicitly account for the influence of buoyancy. For this case, $p = 1$ and C_ψ is of the order of 10^3, as estimated by Mahrt (2000).

Alternatively, Mahrt (1996) suggested considering σ_w as a rough estimation of vertical mixing, without specific attention to whether the origin is due to either wind shear or buoyancy. The variance of vertical velocity can be described in terms of the relationship (Højstrup, 1982),

$$\sigma_w^2 = a u_*^2 + b w_*^2 \tag{10}$$

where w_* is the Deardorff convective velocity scale. Thus, the stability parameter used in this case $\psi = \sigma_w$ (with $p = 2$ and $C_\psi = 2$) generalizes the application of the blending height formulation to shear-driven convective conditions.

Mahrt (2000) uses Eq. (9) to estimate the minimum horizontal scale of the surface heterogeneity that would influence the airborne measurements at the mean observation level $\overline{z}_{\mathrm{obs}}$,

$$L_{\mathrm{blend}} = \frac{1}{C_\psi}\left(\frac{\overline{u}}{\psi}\right)^p \overline{z}_{\mathrm{obs}} = L_{\mathrm{het}} \frac{\overline{z}_{\mathrm{obs}}}{z_{\mathrm{blend}}} \tag{11}$$

with L_{blend} taking different values depending on the stability parameter used. If (for our study) $L_{\text{lake}} = L_{\text{het}} > L_{\text{blend}}$, then the lake is expected to exert a heterogeneity signal on the atmosphere at the observation level.

The concept of a blending height is discussed controversially in literature for strong convective conditions since the largest eddies transport the surface properties up to the CBL top. Raupach and Finnigan (1995) proposed a formulation for the maximum horizontal scale of surface heterogeneity L_{Rau}, for which influence in the CBL is confined to depths much smaller than the boundary-layer height z_i,

$$L_{\text{Rau}} = C_{\text{Rau}} \frac{\overline{u}}{w_*} z_i \tag{12}$$

where C_{Rau} is a non-dimensional coefficient in the order of 1 (Mahrt, 2000). Since the mixing time scale in the CBL is defined as z_i/w_*, L_{Rau} can be interpreted as the horizontal distance covered by the flow during the mixing time scale.

The length scale of the lake L_{lake} is estimated by using the geometrical length of that portion of the leg over the lake surface. This length varies depending on the flight track orientation, since the lake in the east-west direction is five times smaller than in the north-south axis. Hence, the horizontal length scale L_{lake} ranges between 1.5 km and 2 km for all flights. Figure 12 shows the ratio of L_x/L_{lake} versus the leg-averaged wind speed $\overline{u}$ according to Mahrt (2000), where L_x is one of the three possible formulations of L_{blend}:

1. The near-neutral case ($L_{\text{blend}} = L_{\text{n}}$),

$$L_{\text{n}} = C_{\text{n}} \left(\frac{\overline{u}}{u_*} \right)^2 \overline{z}_{\text{obs}} \; , \tag{13}$$

   where C_{n} is 0.6.

2. The modified case ($L_{\text{blend}} = L_{\text{b}}$) after considering the surface heat flux ($\overline{w'\theta'_{sfc}}$) is

$$L_{\text{b}} = C_{\text{b}} \frac{\overline{u}\,\overline{\theta}}{\overline{w'\theta'_{sfc}}} \overline{z}_{\text{obs}} \; , \tag{14}$$

   where C_{b} is $3.1 \cdot 10^{-3}$.

3. The generalized case with σ_w and $C_{\text{w}} = 0.5$ ($L_{\text{blend}} = L_{\text{w}}$) is

$$L_{\text{w}} = C_{\text{w}} \left(\frac{\overline{u}}{\sigma_w} \right)^2 \overline{z}_{\text{obs}} \; . \tag{15}$$

Results for L_{Rau} (Eq. 12) for the cases in which the CBL depth z_i was available are also included as is L_{ibl} which is explained later. The CBL depth was measured by a Lidar or Radiosonde. Further details can be found in Beyrich and Mengelkamp (2006). The horizontal gray line at $L_x/L_{\text{lake}} = 1$ indicates where the geometrical length scale L_{lake} is equal to the minimum length scale L_x. That means, when the ratio L_x/L_{lake} is smaller than one, the geometrical length scale of the lake L_{lake} is larger than the minimum required horizontal length scale of the surface heterogeneity, which is needed to influence the airborne measurements at the mean observation level. All length scales increase for larger wind speeds. Larger wind speeds reduce the Lagrangian time that the flow spends over a particular surface feature. Hence, a longer horizontal length scale of this surface feature is required to achieve a similar depth of influence (Mahrt, 1996). Only for very few cases, $L_{\text{n}}/L_{\text{lake}}$ and $L_{\text{b}}/L_{\text{lake}}$ are less than unity, generally for mean wind speeds $\overline{u} < 3$ m s^{-1}. Only $L_{\mathrm{w}}/L_{\mathrm{lake}}$ shows values smaller than unity, for almost all the cases (except for those legs with the largest wind speeds).

As mentioned in the introduction, the convective length scale L_{Rau} indicates the size of heterogeneity that are supposed to influence the entire boundary layer. L_{Rau} depends on the intensity of convection (represented by the Deardorff velocity scale w_*), the boundary-layer depth z_i and the mean horizontal wind speed $\overline{u}$ (see Eq. 12). The results for L_{Rau} indicate a behaviour similar to L_{n} and L_{b}, with $L_{\mathrm{Rau}} > L_{\mathrm{lake}} \sim 2$ km for larger wind speeds ($\overline{u} > 4$ m s^{-1}). Under these wind conditions, horizontal convective mixing prevents the lake influence from extending up to the boundary-layer height. However, previous studies over the same area show that the sensible heat flux remains very small throughout the entire CBL over lake Scharmützelsee (Bange et al, 2006), and it only matches with the surrounding area at the upper ABL, where sensible heat flux over land is small (Sühring and Raasch, 2013). Strunin et al (2004) found that L_{Rau} had to be complemented with a ratio between shear stress and buoyancy flux at 100 m to successfully determine the ability of a CBL for horizontal mixing. In the present study, the lack of iterative passes at higher altitudes precludes a more robust analysis for addressing the vertical extension of the lake.

Flows over surface discontinuities can develop local internal boundary layers (IBL) downstream, when the changes of surface properties are sharp enough or the scale of the surface heterogeneity is large. When a local IBL develops, Mahrt (1996) estimated its maximum depth z_{ibl} with scaling arguments as

$$z_{\mathrm{ibl}} = C_{\mathrm{ibl}} \frac{\sigma_w}{\overline{u}} L_{\mathrm{het}} \,, \tag{16}$$

where C_{ibl} was found to be 0.15 (Mahrt, 2000). Similarly to what we have applied for the blending-height parameterizations, it is possible to rewrite (16) in order to calculate the minimum length scale that would generate a local IBL with a depth similar to the observation level:

$$L_{\mathrm{ibl}} = \frac{1}{C_{\mathrm{ibl}}} \left(\frac{\overline{u}}{\sigma_w} \right) \overline{z}_{\mathrm{obs}} \,. \tag{17}$$

Note that L_{ibl} is very similar to L_{w}, although with a linear dependence on the ratio $\overline{u}/\sigma_w$. Figure 12 shows the values estimated for our dataset, with minimum scales larger than L_{w}. Therefore, larger heterogeneity scales are generally necessary in order to detect the development of an IBL at a given reference level.

In our dataset, we are able to see a slight drop in the potential temperature but none of the legs analysed identify a clear change in the mean variables, as we would expect when entering an IBL. Thus, we can say that a well defined IBL, which is in equilibrium with the underlying surface cannot be clearly identified with our observations according to Eq. 17, or alternatively the flow adjusts to the new surface without the formation of an IBL. These observations are in accordance with the LES study from Maronga et al (2014). They could identify for the LITFASS-2003 case study that blending effects occur above several tens of metres above the ground for temperature fluctuation.

The fact that the IBL top is not well defined in the layer between 60 and 100 m may suggest that the scales estimated for the top of the IBL in (16) are valid. As a consequence, between 60 and 100 m, the influence of the underlying surface can only be detected in the second-order moments of the variables. Following this argumentation, we would expect that the lowest flight legs were performed within a layer between the top of the IBL (for those cases where it was generated) and the blending height. In this layer, the surface influence would gradually vanish with altitude. One should keep in mind, that the various scaling derivations were intended more as qualitative arguments based in part on linear theory (Mahrt, 2000). Therefore, quantitative comparisons of the length scales formulations is extremely difficult with more complex atmospheric flow as they occur over heterogeneous terrain.

5 Horizontal propagation of the lake influence

The above scaling estimates neglect important spatial variations of the stability parameters ψ and other variables. Therefore they do not attempt to describe the power-law dependence on the downstream distance that generally applies for the generation of an IBL (Garratt, 1990; Józsa et al, 2007). The current dataset shows that the influence of the lake on the distribution of the standard deviation of potential temperature is commonly shifted downstream. An attempt to characterize this horizontal shift is addressed by analysing the correlation between the atmospheric response (characterized by σ_θ) and the surface radiation temperature T_0. In this case, we have considered the 1-km overlapping windows for each leg below 100 m, as a spatial series of σ_θ and T_0. We then calculated the cross-correlation function,

$$\rho(S) = \frac{\mathrm{cov}\left[\sigma_\theta(x+S), T_0(x)\right]}{\left(\mathrm{var}[\sigma_\theta]\right)^{1/2} \cdot \left(\mathrm{var}[T_0]\right)^{1/2}}\ , \tag{18}$$

where $S = j \cdot \Delta s$ represents the spatial lag, $\Delta s = 250$ m is the fixed horizontal distance between two consecutive overlapping windows along the leg and $j \in (-10, 10)$. In contrast to the one-point correlation analysis, the cross-correlation function allows us to analyse the spatial displacement of the vertical transport by horizontal advection.

Figure 13 shows the cross-correlation functions for the three legs of STI09 flight performed below 100 m. Further two more legs ST03 and NT13 have been added from STI09 which have not been presented before, but that also cross the lake in a similar way. These two legs have the same track and height than MT02, but are located more to the north (NT13) and to the south (ST03) over the lake. The maximum value of $\rho(S)$ occurs for a spatial lag S between 0.75 and 0.50 km, with the negative sign indicating that the maximum correlation is shifted downstream to the west, since there was predominant easterly wind. The leg MT12 represents one exception to these results, with a function ρ that exhibits a plateau within lags $S = \pm 1.5$ km. A positive correlation is expected since the drop in σ_θ occurs for smaller surface temperatures, as the thermals over these regions are weaker.

The cross-correlation function has been calculated for the rest of cases with a small cross-leg wind component ($u_{\mathrm{cross}}/\overline{u} < 0.5$). A total of 12 legs met this condition, and for 8 of them a maximum correlation of $\rho_{\max} > 0.4$ was obtained. All these cases show the maximum cross-correlation for a corresponding downstream spatial lag.

If we consider $(\sigma_w/\overline{u})$ as a qualitative ratio of the strength of the vertical mixing to the horizontal advective speed, it is possible to relate the spatial lag $S_{\max}$ of the maximum of the correlation function with the leg-averaged wind along the leg direction $\overline{u}_\parallel$, the leg-averaged standard deviation of vertical wind σ_w and the observational height $\overline{z}_{\mathrm{obs}}$. Based on Eq. 17, we get:

$$S_{\max} \sim \frac{1}{C_\delta}\left(\frac{\overline{u}_\parallel}{\sigma_w}\right)\overline{z}_{\mathrm{obs}} = \delta x_{\mathrm{par}}, \tag{19}$$

where we call this relation the parameterized distance δx_{par}. C_δ is a non-dimensional coefficient which has to be defined. If this relation (Eq. 19) is reasonable $S_{\max}$ and δx_{par} should be equal. Figure 14 shows the absolute difference between δx_{par} and $S_{\max}$ for varying C_δ. In order to obtain C_δ for different conditions, we calculated this difference considering (i) the whole dataset (34 legs), (ii) a subset with only those legs with $\rho_{\max} > 0.4$ (12 legs) and finally (iii) a reduced subset of legs with $\rho_{\max} > 0.4$ and low cross-wind ($u_{\mathrm{cross}}/\overline{u} < 0.5$, 8 legs). The smallest difference is obtained for the latter subset, with a value of $C_\delta \approx 0.4$. The subset of legs with $\rho_{\max} > 0.4$ also show a minimum close to $C_\delta \approx 0.4$, however the absolute difference is higher. A suitable value for parameter C_δ can not be determined when all legs are considered since a minimum value is not found.

For the neutral case, Horst and Weil (1992) found that the level of maximum influence $\overline{z}$ of a given upstream unit surface point source is proportional to the downstream distance δx through the relation

$$\delta x = \frac{\overline{z}}{\kappa\sqrt{C_D}} = \frac{1}{\kappa}\frac{\overline{u}}{u_*}\overline{z}, \tag{20}$$

where $C_D = (u_*/\overline{u})^2$ is the drag coefficient and $\kappa = 0.40$ is the von-Kármán constant. In our case we have to assume that the lake acts like a unit surface point source. That means we consider the lake as one point with no horizontal extension, from where the spatial distance of a footprint in the boundary layer is calculated. We have seen in previous sections, that for our study, σ_w is a better scaling variable for turbulence compared to u_*. σ_w is needed to calculate the length scale L_w. Only with this length scale L_w, the geometrical length of the lake is large enough in order to show a footprint at the observation height of the lake for the most of our cases, including higher wind speeds (see Fig. 12.)

Thus, relation (20) with σ_w instead of turns into expression (19), with a value of C_δ close to κ. The parametrization of (19) with $C_\delta = 0.4$ is displayed for the two different legs (LIT13 and LIT14) in Fig. 10. The vertical black dashed lines indicate the lake boundaries shifted downstream by the distance δx_{par} following the parameterization. Since the parametrization depends on the horizontal wind speed and on the vertical mixing, the distance of the black dashed lines respect to the lake boundaries is different for both flights (LIT13 and LIT14) as weather conditions were also different. The segment of the lake with the minimum of the σ_θ should be located within the black dashed lines for both cases. For LIT14 the drop of the σ_θ is in between the parametrized distance. LIT13 is a good example for showing that not all cases follow the parametrization. However, it is necessary to use the entire dataset in order to test the validity of the approach given by Eq. 19. We have identified the region with a maximum drop in σ_θ over the vicinity of the lake for 29 legs by a computer algorithm detection (as explained in Sect. 3.6). The detection of a drop in σ_θ is satisfactorily for most cases (indicated by open circles in Fig. 10).

In the previous section 3.6, we defined the horizontal distance between the geometrical centre of that region where the drop of σ_θ occurs and the centre of the lake, as the observed mean propagation distance of the lake influence δx_{obs} at the leg height $\overline{z}_{\mathrm{obs}}$.

If expressions of Eq. 19 is valid, the parameterized distance δx_{par} should fit to the observed one δx_{obs}. In Fig. 15 the difference $\mid \delta x_{\mathrm{obs}} - \delta x_{\mathrm{par}} \mid$ is plotted versus the mean wind speed $\overline{u}$. The discrepancy between the observed and parameterized shifts is smaller than the spatial lag between two consecutive overlapping windows (250 m) for 15 cases. Hence, 55% of the cases exhibit an observed horizontal shift similar to the parametrized results from Eq. 19. However, the parametrization δx_{par} does not hold for all cases. It tends to fail for situations with large wind speeds.

6 Conclusion

The influence of an intermediate-scale lake on airborne measurements taken below 100 m in a CBL has been analysed for 34 flight legs flown during two consecutive field campaigns in the summer of 2002 and 2003. Several first-order and second-order statistics were evaluated in order to check if an lake influence is apparent in the lower CBL in the vicinity of the lake. The spatial variability for mean quantities is not very significant. Although there are some hints that our analysed data indicate a cooling over the lake at 100 m above ground and that we can distinguish between a drier atmosphere over the lake compared to the moister air over forest.

The second-order moments related to potential temperature (σ_θ) exhibit a clear decrease in the vicinity of the lake at the airborne observation height. Unfortunately, only one flight of the selected dataset contained consecutive passes along the same leg during same environmental conditions and hence a low sampling error. The flight showed that the observed variances of σ_θ are reduced significantly over the lake. But also the remaining flights, each with different environmental conditions, showed reduced σ_θ in 33 out of 34 flight legs. Although due the lack of iterative passes the theoretical sampling error is in the same order as the measurement value, the persistence of a drop in σ_θ for most of the flights in the downstream propagation of the lake is significant. Most likely, the lack of thermals above a cool surface favours such a drop for theses parameters and their random variability. Second-order moments of humidity and vertical wind, however, did not identify the underlying lake, at least in our study.

The fact that, a slight drop is seen in the potential temperature but none of the legs analysed identify a clear change in the mean variables, as we would expect when entering an IBL, suggest that a well defined IBL is not observed in our data set. Therefore, an IBL which should be as well in equilibrium with the underlying surface cannot be clearly identified with our observations according to Eq. 17. It seems to be more likely, that the flow adjusts to the new surface, which is indicated by the decrease of variance of temperature over the lake, but without the formation of an IBL.

Several length scales of surface heterogeneity were calculated following previous studies of Mahrt (2000) and Bange et al (2006). These scales consider different parameters depending on the stability conditions of the flow. Only the scale that considers the variance of vertical velocity or a velocity scale was compatible with our observations. Probably the variety of buoyancy conditions in our dataset (which includes days with a weak surface heat flux and strong winds together with days with strong convection) requires a stability parameter able to describe the vertical mixing induced by both wind shear and thermal heating in order to fit to all conditions during our flight experiment. In addition, the application of a convective scale for those cases where the boundary-layer depth was known, indicates that the 2 km wide lake could affect the lower CBL for wind speeds below 4 m s^{-1}.

Finally, the downstream propagation of the lake influence has been addressed by calculating the cross-correlation function between the surface radiative temperature and the variance of potential temperature for the entire leg. Although a clear relationship between the spatial lag of the maximum correlation and the horizontal advective speed could only be identified for 8 cases, this relation indicates promising results when it is applied solely to the lake influence. After developing a system of that automatically detects the mean horizontal shift of the lake influence, 55% of the cases exhibit an observed horizontal shift similar to the simple parametrization of Eq. 19.

Atmospheric flow is complex. Therefore a quantitative comparison of the various length scales derivations and downstream parametrizations which are based on linear theory is difficult. In future flight experiments, we suggest simultaneous flights with at least three research aircraft, at three different levels above a discontinuity, performing repeated legs. Ideally this could be done using research unmanned air vehicles (UAV) (van den Kroonenberg et al, 2012; Wildmann et al, 2014). By using UAV, also the flight altitude can be maintained with a much higher precision ($\pm$1m) compared to a manned helicopter.

Acknowledgments

The measurements were performed during the LITFASS-2003 experiment, a field experiment within the framework of the EVA_GRIPS project (Evaporation at grid / pixel scale). EVA_GRIPS was funded by the German Federal Ministry of Education and Research (BMBF) as a part of the German climate research program (DEKLIM) under the contract no. 01LD0103. Andreas Lang is acknowledged for its preliminary analysis of the current experimental dataset for his BSc Thesis.

References

Avissar R, Schmidt T (1998) An evaluation of the scale at which ground-surface heat flux patchiness affects the convective boundary layer using large-eddy simulations. Journal of the Atmospheric Sciences 55(16):2666–2689

Bange J, Roth R (1999) Helicopter-borne flux measurements in the nocturnal boundary layer over land - a case study. Bound-Layer Meteorol 92:295–325

Bange J, Beyrich F, Engelbart DAM (2002) Airborne measurements of turbulent fluxes during LITFASS-98: Comparison with ground measurements and remote sensing in a case study. Theor Appl Climatol 73:35–51

Bange J, Spieß T, Herold M, Beyrich F, Hennemuth B (2006) Turbulent fluxes from helipod flights above quasi-homogeneous patches within the litfass area. Boundary-layer meteorology 121(1):127–151

Bange J, Esposito M, Lenschow DH (2013) Airborne Measurements for Environmental Research – Methods and Instruments, Wiley, chap 2: Measurement of Aircraft State, Thermodynamic and Dynamic Variables, p 641 pp

Beyrich F, Mengelkamp HT (2006) Evaporation over a heterogeneous land surface: EVA-GRIPS and the LITFASS-2003 experiment – an overview. Bound-Layer Meteorol 121(73):5–32

Beyrich F, Herzog HJ, Neisse J (2002) The LITFASS project of DWD and the LITFASS-98 experiment: The project strategy and the experimental setup. Theor Appl Climatol 1-2(73):3–18

Beyrich F, Leps JP, Mauder M, Bange J, Foken T, Huneke S, Lohse H, Lüdi A, Meijninger WM, Mironov D, et al (2006) Area-averaged surface fluxes over the LITFASS region based on eddy-covariance measurements. Boundary-layer meteorology 121(1):33–65

Garratt J (1990) The internal boundary layer – a review. Bound-Layer Meteorol 50:171–203

Göckede M, Mauder M, Foken T (2004) Qualitätsbegutachtung komplexer mikrometeorologischer Messstationen im Rahmen des VERTIKO-Projekts. Univ. Bayreuth, Abt. Mikrometeorologie

Grossmann S, Lohse D, L'vov V, Procaccia I (1994) Finite size corrections to scaling in high reynolds number turbulence. Physical review letters 73(3):432

Hadfield M, Cotton W, Pielke R (1991) Large-eddy simulations of thermally forced circulations in the convective boundary layer. part i: A small-scale circulation with zero wind. Boundary-Layer Meteorology 57(1-2):79–114

Hadfield M, Cotton W, Pielke R (1992) Large-eddy simulations of thermally forced circulations in the convective boundary layer. part ii: The effect of changes in wavelength and wind speed. Boundary-Layer Meteorology 58(4):307–327

Højstrup J (1982) Velocity spectra in the unstable planetary boundary layer. J Atmos Sci 39:2239–2248

Horst T, Weil J (1992) Footprint estimation for scalar flux measurements in the atmospheric surface layer. Boundary-Layer Meteorology 59(3):279–296

Huang HY, Margulis SA (2009) On the impact of surface heterogeneity on a realistic convective boundary layer. Water Resources Research 45(4)

Józsa J, Milici B, Napoli E (2007) Numerical simulation of internal boundary-layer development and comparison with atmospheric data. Bound-Layer Meteorol 123:159–175

van den Kroonenberg AC, Martin S, Beyrich F, Bange J (2012) Spatially-averaged temperature structure parameter over a heterogeneous surface measured by an unmanned aerial vehicle. Bound-Layer Meteorol 142:55–77

Lenschow D, Mann J, Kristensen L (1994) How long is long enough when measuring fluxes and other turbulence statistics? Journal of Atmospheric and Oceanic Technology 11(3):661–673

Lenschow DH, Stankov BB (1986) Length scales in the convective boundary layer. J Atmos Sci 43:1198–1209

Letzel MO, Raasch S (2003) Large eddy simulation of thermally induced oscillations in the convective boundary layer. Journal of the atmospheric sciences 60(18):2328–2341

Lumley L, Panofsky H (1964) The Structure of Atmospheric Turbulence. John Wiley & Sons, 239 pp.

Mahrt L (1996) The bulk aerodynamic formulation over heterogeneous surfaces. Bound-Layer Meteorol 78:87–119

Mahrt L (2000) Surface heterogeneity and vertical structure of the boundary layer. Bound-Layer Meteorol 96:33–62

Mann J, Lenschow DH (1994) Errors in airborne flux measurements. Journal of Geophysical Research: Atmospheres (1984–2012) 99(D7):14,519–14,526

Maronga B, Raasch S (2013) Large-eddy simulations of surface heterogeneity effects on the convective boundary layer during the LITFASS-2003 experiment. Bound-Layer Meteorol 146:17–44

Maronga B, Hartogensis OK, Raasch S, Beyrich F (2014) The effect of surface heterogeneity on the structure parameters of temperature and specific humidity: a large-eddy simulation case study for the litfass-2003 experiment. Boundary-Layer Meteorology 153(3):441–470

Mengelkamp HT, Beyrich F, Heinemann G, Ament F, Bange J, Berger F, Bösenberg J, Foken T, Hennemuth B, Heret C, et al (2006) Evaporation over a heterogeneous land surface: the EVA-GRIPS project. Bulletin of the American Meteorological Society 87(6):775–786

Panofsky H, Larko D, Lipschutz R, Stone G, Bradley E, Bowen AJ, Højstrup J (1982) Spectra of velocity components over complex terrain. Quarterly Journal of the Royal Meteorological Society 108(455):215–230

Raabe A, Arnold K, Ziemann A, Beyrich F, Leps JP, Bange J, Zittel P, Spiess T, Foken T, Göckede M, et al (2005) STINHO–structure of turbulent transport under inhomogeneous surface conditions–part 1: The micro-α scale field experiment. Meteorologische Zeitschrift 14(3):315–327

Raupach RR, Finnigan JJ (1995) Scale issues in boundary-layer meteorology: surface energy balances in heterogeneous terrain. Hydro Proc 9:589–612

Sahlée E, Rutgersson A, Podgrajsek E, Bergström H (2014) Influence from surrounding land on the turbulence measurements above a lake. Boundary-layer meteorology 150(2):235–258

Samuelsson P, Kourzeneva E, Mironov D (2010) The impact of lakes on the european climate as stimulated by a regional climate madel. Boreal environment research 15(2)

Shao Y, Hacker JM (1990) Local similarity relationships in a horizontally inhomogeneous boundary layer. Boundary-Layer Meteorology 52(1-2):17–40

Shao Y, Hacker JM, Schwerdtfeger P (1991) The structure of turbulence in a coastal atmospheric boundary layer. Quarterly Journal of the Royal Meteorological Society 117(502):1299–1324

Strunin MA, Hiyama T, Asanuma J, Ohata T (2004) Aircraft observations of the development of thermal internal boundary layers and scaling of the convective boundary layer over non-homogeneous land surfaces. Bound-Layer Meteorol 111:491–522

Stull R (1988) An Introduction to Boundary Layer Meteorology. Kluwer Academic Publisher, Dordrecht

Sühring M, Raasch S (2013) Heterogeneity-induced heat-flux patterns in the convective boundary layer: Can they be detected from observations and is there a blending height?—A Large-Eddy Simulation study for the LITFASS-2003 experiment. Bound-Layer Meteorol 148:309–331

Wildmann N, Hofsäß M, Weimer F, Joos A, Bange J (2014) MASC–a small remotely piloted aircraft (RPA) for wind energy research. Advances in Science and Research 11(1):55–61

Wood N, Mason P (1991) The influence of stability on effective roughness lengths for momentum and heat transfer. Q J R Meteorol Soc 117:1025–1056

7 Tables, Plots

Table 1: List of selected flights. All flights took place in 2003 except STI09 which was in 2002. Ws is the wind speed. Local time is UTC + 2 hours. Times are the entire flight time.

Flight code	Date	Time (UTC)	Heights of legs (m)	Weather (Clouds)	Wind dir (°)	Ws (m s^{-1})
IBL-lake						
STI09	09.07	1320–1500	70, 80, 90, 180, 280	2/8 Ci	150	6.0
LIT13	13.06	1312–1412	86, 472, 603, 742, 922	5/8 Ci	300	8.0
LIT14	14.06	0922–1020	86, 472, 603, 742, 922	7/8 Ci, 3/8 Cu	280	4.0
North box						
LIT24	24.05	1312–1405	100, 400, 700	4-6/8 Ci	141	6.3
LIT25	25.05	0929–1040	100, 400, 700	1/8 Ci	142	2.2
LIT07	07.06	0953–1050	100, 400, 700	1/8 Ci	151	3.3
E-W grids						
LIT28	28.05	1203–1307	100	3-4/8 Ci	28-54	5.0
LIT03	03.06	1122–1225	100	4/8 Ci	92-148	2.6
LIT04	04.06	1216–1321	100	3-6/8 Ci	125-159	5.0
LIT06	06.06	1132–1239	100	2/8 Ci	260-310	5.5
LIT10	10.06	0906–1010	100	5/8 Ci	113-175	3.0
LIT12	12.06	0923–1026	100	2-3/8 Ci	274-348	4.0
LIT13	13.06	0940–1041	100	3-2/8 Ci	300	4.3
LIT17	17.06	1235–1333	100	3/8 Cu 4/8 Ci	68-168	2.8

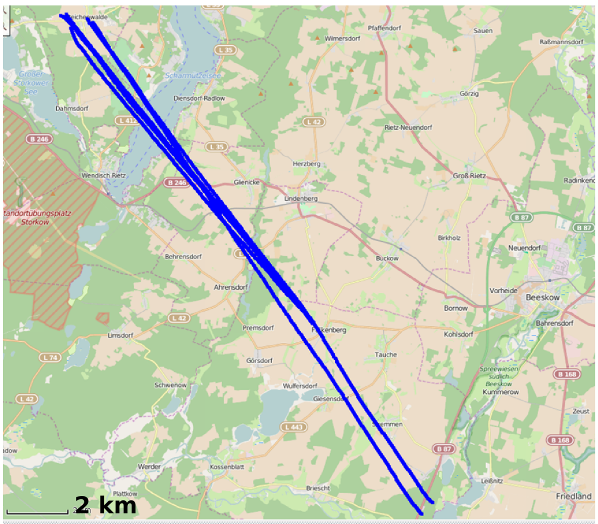

(a) Flight-tracks of IBL-lake flights (STI09, LIT13, LIT14)

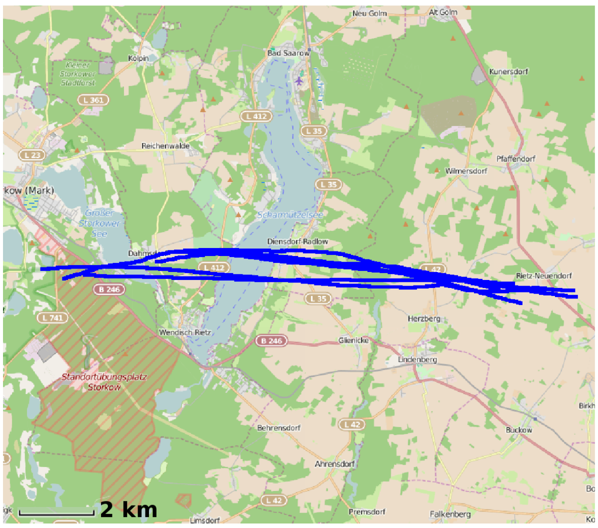

(b) Flight-tracks of LITFASS2003 flights (Northbox) and (E-W grids)

Figure 1: Flight-tracks (blue lines) representative of those flights that cross the lake Scharmültzelsee (a) following the mean wind (STI09, LIT13 and LIT14) or (b) in the east-west direction at different heights or over different sections of the lake (the rest of flights, see Tab. 1). Green areas refer to forest surfaces, blue to water and beige to farmland. Hatching areas indicate military zones. Source. Open Street Map.

Table 2: Chronology of the legs performed during STI09 flight. Error in the Height column represents the standard deviation. Local time is UTC + 2 hours. Times report the analyzed flight period.

Time (UTC)	leg number (position)	Height (m)	θ average (K)	Wind dir (°)	Wind speed (m s^{-1})	leg-parallel wind speed (m s^{-1})
1327–1333	MT 02	83 ± 17	303.5	143	6.3	6.3
1344–1352	MT 04	170 ± 26	303.7	142	7.1	7.1
1402–1409	MT 06	282 ± 28	303.9	145	6.6	6.6
1438–1444	MT 12	66 ± 15	304.5	162	5.8	5.4
1500–1506	MT 16	68 ± 12	304.7	162	5.5	5.1

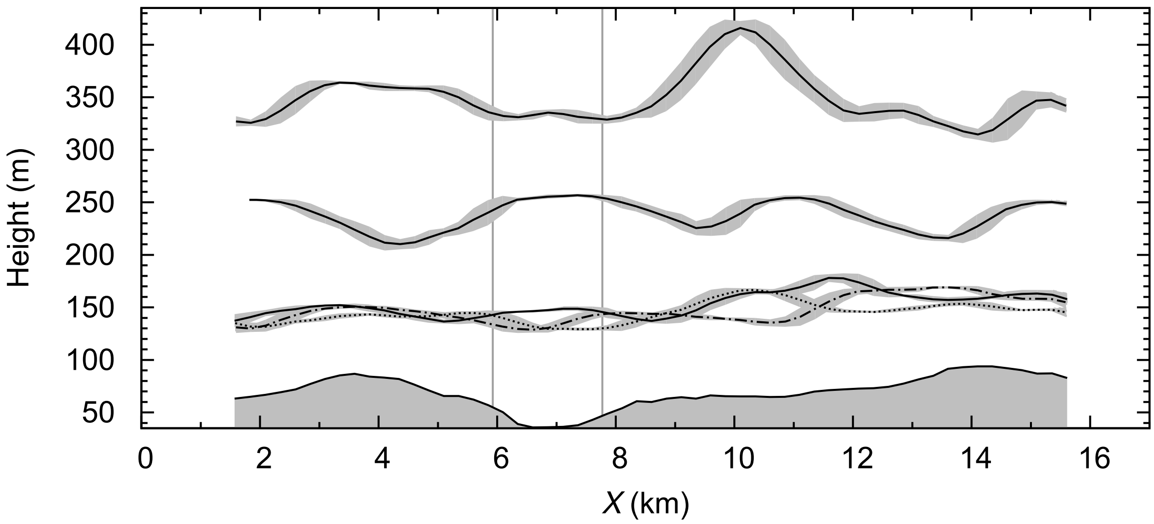

Figure 2: Averaged barometric heights along the five middle track (MT) legs performed during the STI09 flight. Shaded areas correspond to the standard deviation of the altitude along the 1-km window. Abscissa shows the distance along the leg, where X is the distance from an arbitrary point at the western edge of the flight paths. The lowest shaded area depicts the 1-km averaged topography. Vertical gray lines indicate lake boundaries.

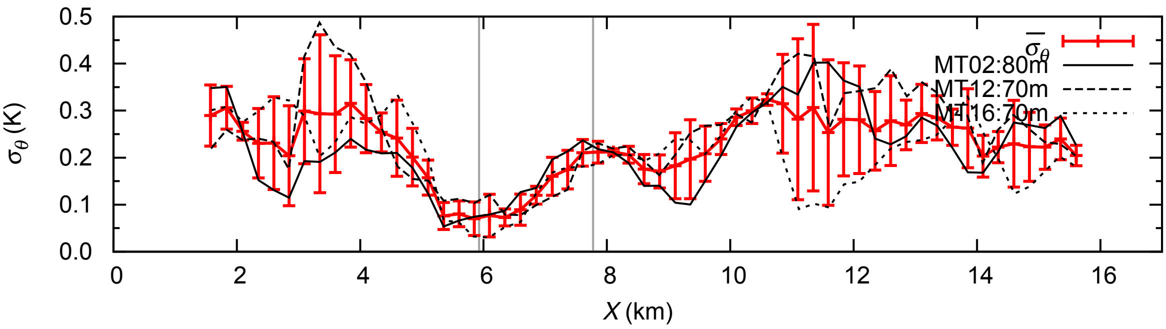

Figure 3: Standard deviation for σ_θ of the three passes at the lowest flight legs MT02, MT12, MT16. The red line indicates the average $\overline{\sigma_\theta}$ of the three legs. Error bars ζ_{σ_θ} mark the sampling error calculated after Eq. 7. Wind blows parallel to the flight direction (from the right side to the left side in the panel). Average wind speed is between 5.5 and 7.1 m s^{-1}. See Table 2 for more information.

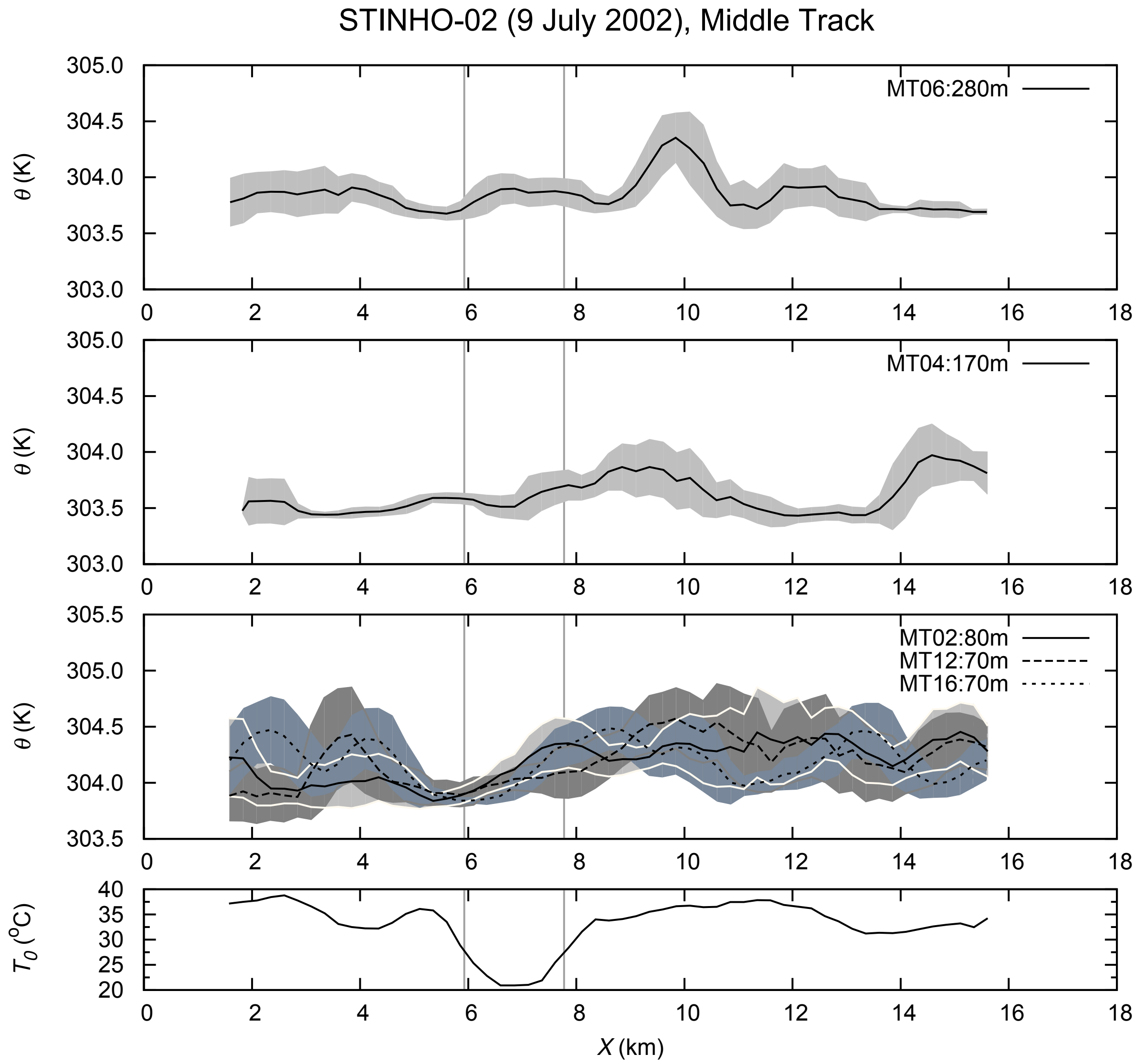

Figure 4: Averaged potential temperature (thick line) and standard deviation (shaded area) for each middle track (MT) leg at 280 m (MT06), at 170 m (MT04) and below 100 m (MT02, MT12, MT16) of STI09 flight. The time variability of the temperature is removed. Lower panel shows the corresponding distribution of the surface temperature measured during the flight leg (MT02). Abscissa and vertical grey lines as in Fig. 2. Wind is blowing parallel to the flight direction (from the right to the left side in the panel). Average wind speed is between 5.5 and 7.1 m s^{-1}. See Table 2 for more information.

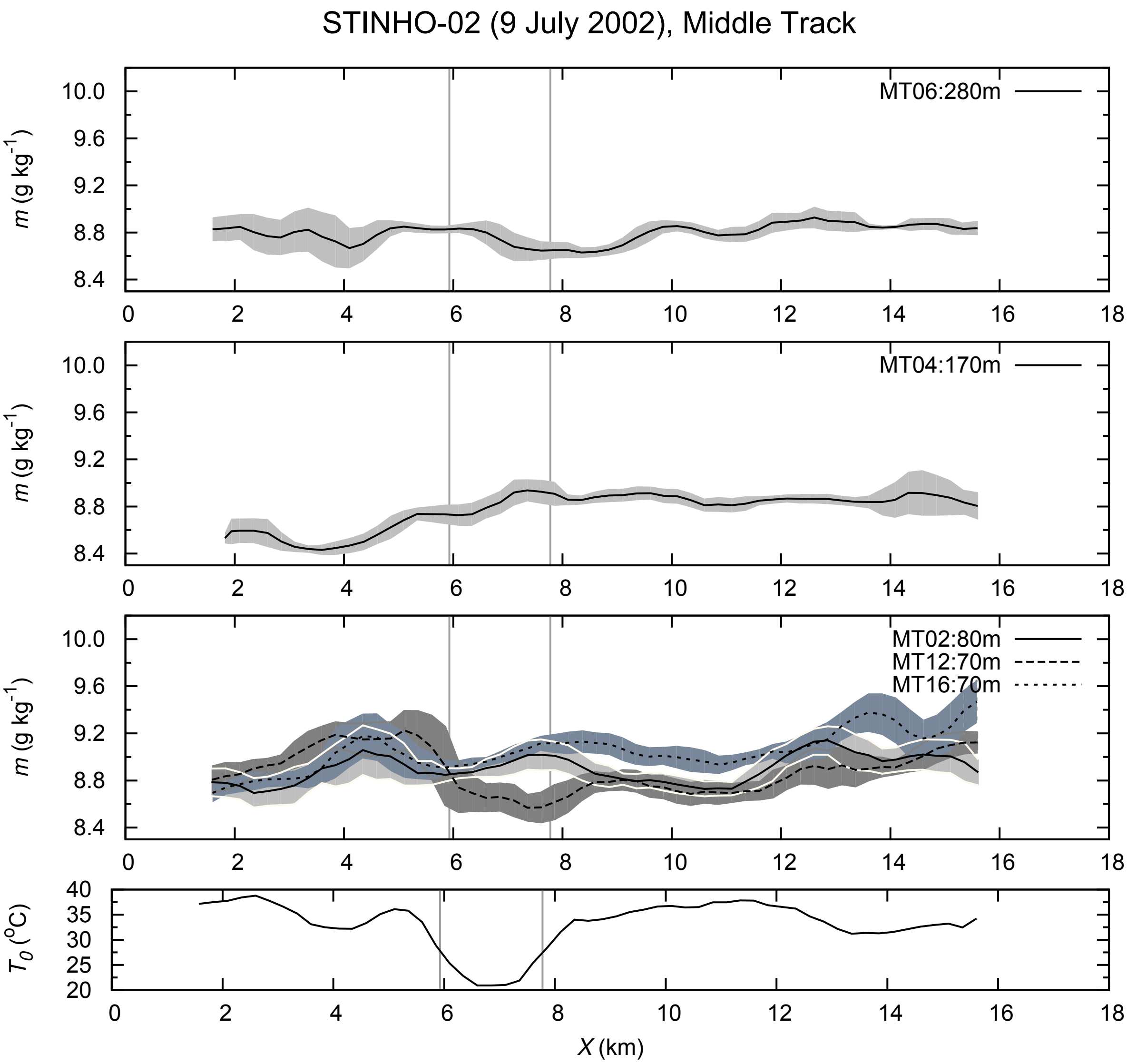

Figure 5: As in Fig. 4 but for water vapor mixing ratio.

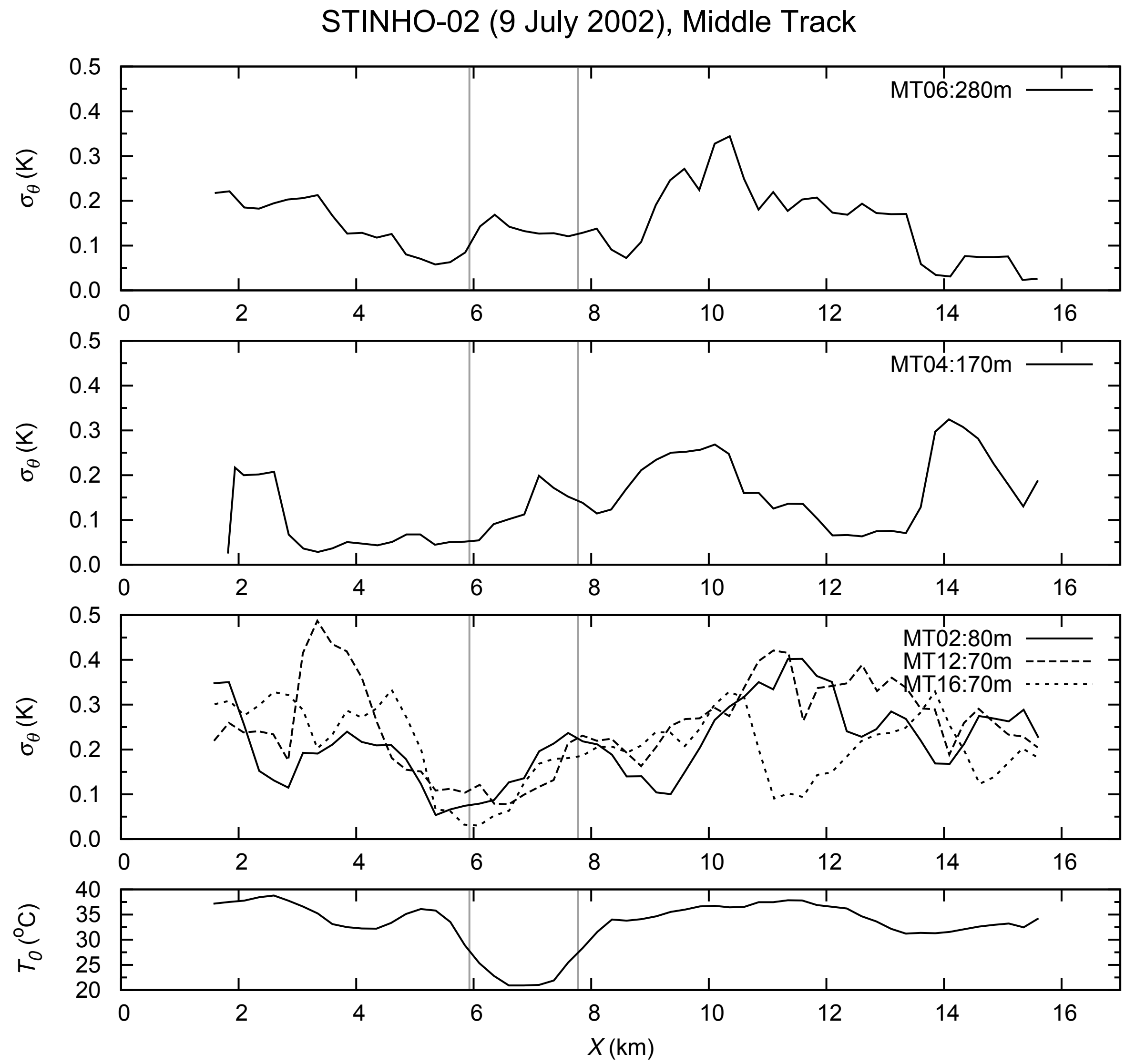

Figure 6: Standard deviation of potential temperature for each middle track (MT) leg at 280 m (MT06), at 170 m (MT04) and below 100 m (MT02, MT12, MT16) of STI09 flight. Data are computed for a window of 1 km width, sequentially marched through the leg by increments of 250 m. Lower panel shows the corresponding distribution of the surface temperature measured during the flight leg (MT02). Wind direction is from the south-east. That means wind is blowing parallel to the flight direction (from the right side to the left side in the panel). Average wind speed is between 5.5 and 7.1 m s^{-1}. See Table 2 for more information.

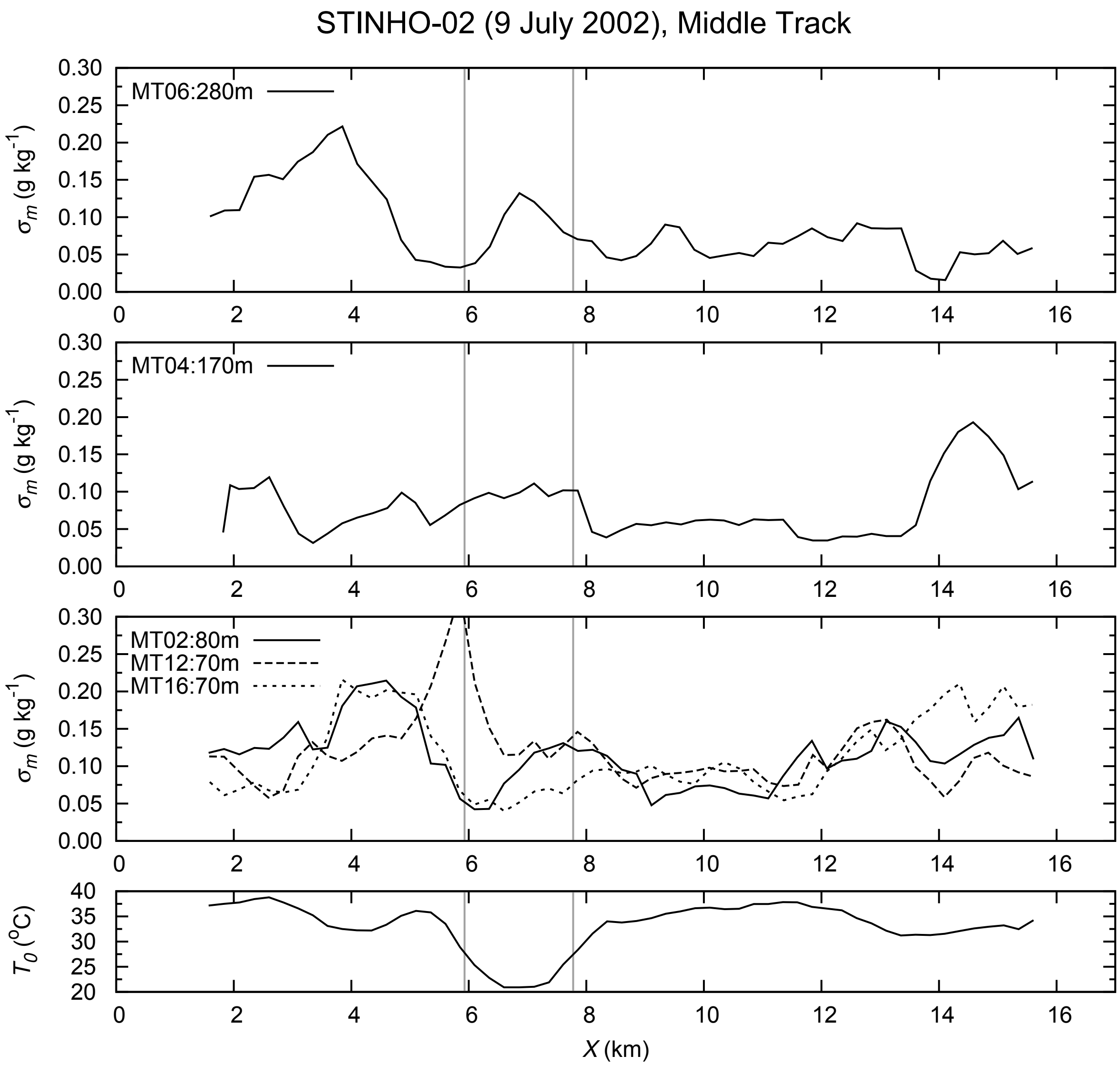

Figure 7: The same as in Fig. 6 but for the water vapor mixing ratio.

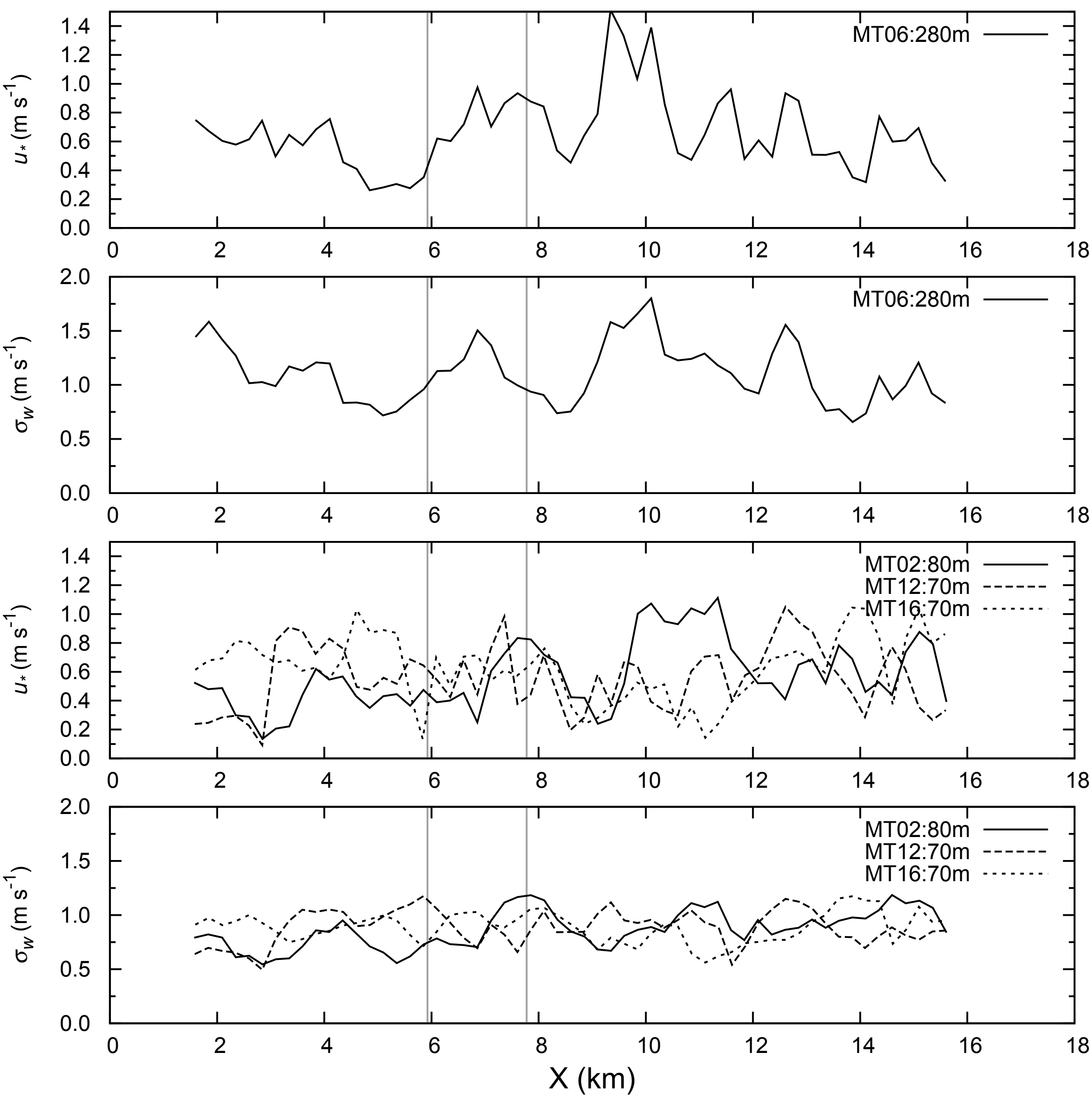

Figure 8: The same as in Fig. 6 but for u_* and σ_w for each middle track (MT) leg at 280 m (MT06), and below 100 m (MT02, MT12, MT16) of STI09 flight.

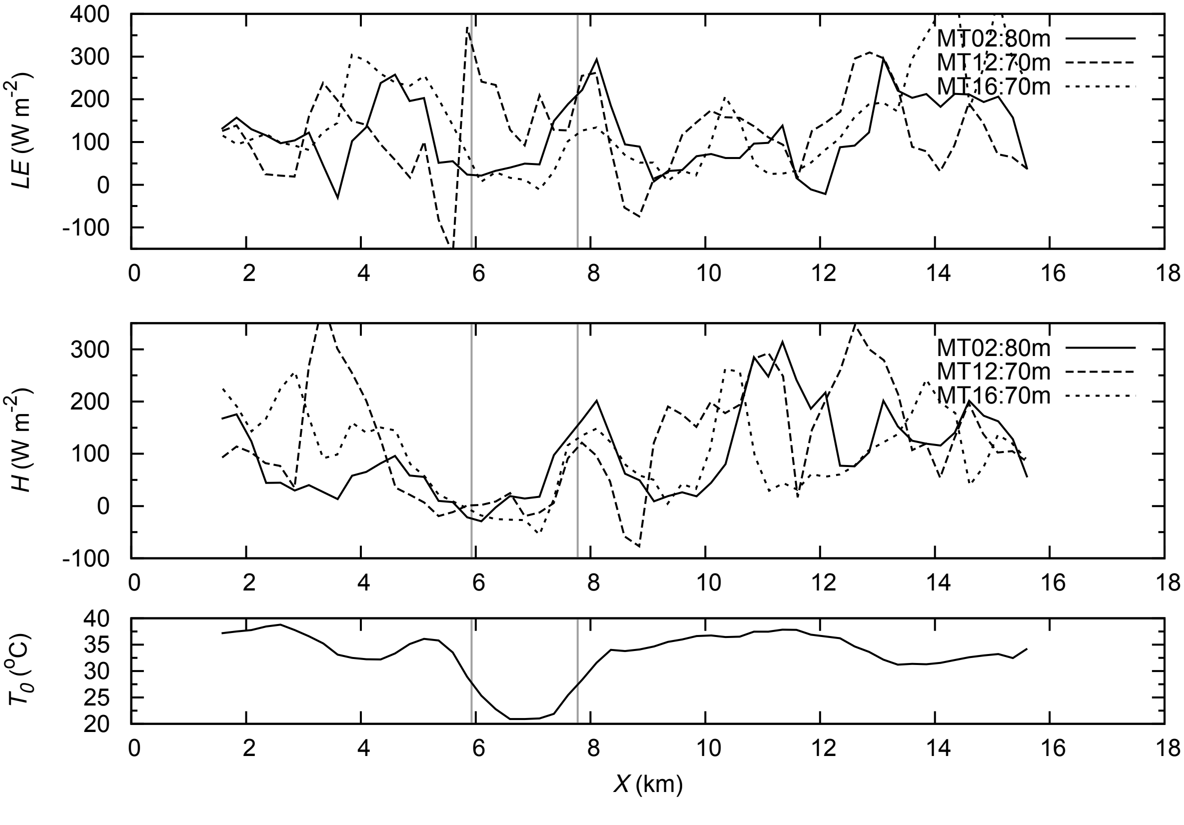

Figure 9: The same as in Fig. 8 but for latent heat flux LE and sensible heat flux H .

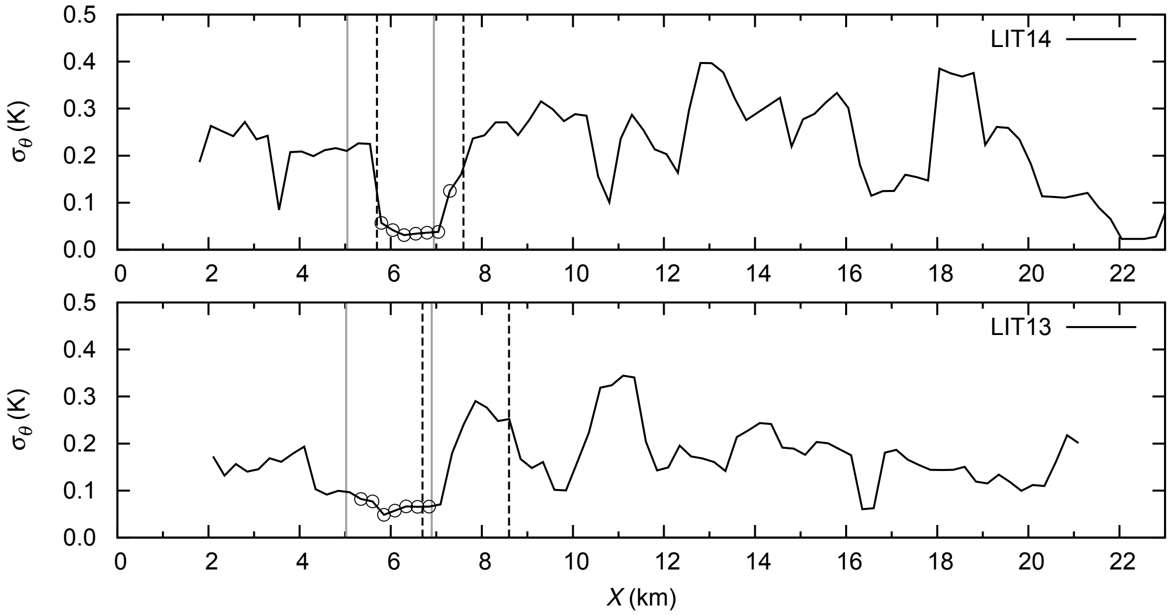

Figure 10: Standard deviation of potential temperature σ_θ for legs LIT14 (top) and LIT13 (bottom). Vertical gray lines indicate the lake boundaries as diagnosed by the surface temperature. Circles indicate the segment of the leg with the lowest values of σ_θ at the vicinity of the lake. This segment has been identified with an automatic algorithm, described at the end of Sect. 3.6. Black dashed lines indicate the segment of the leg where the lake influence should be detected following the parametrization (δx_{par}) developed in Sect. 5 (Eq. 19). Refer to the text (Sect. 3.6) for more informations.

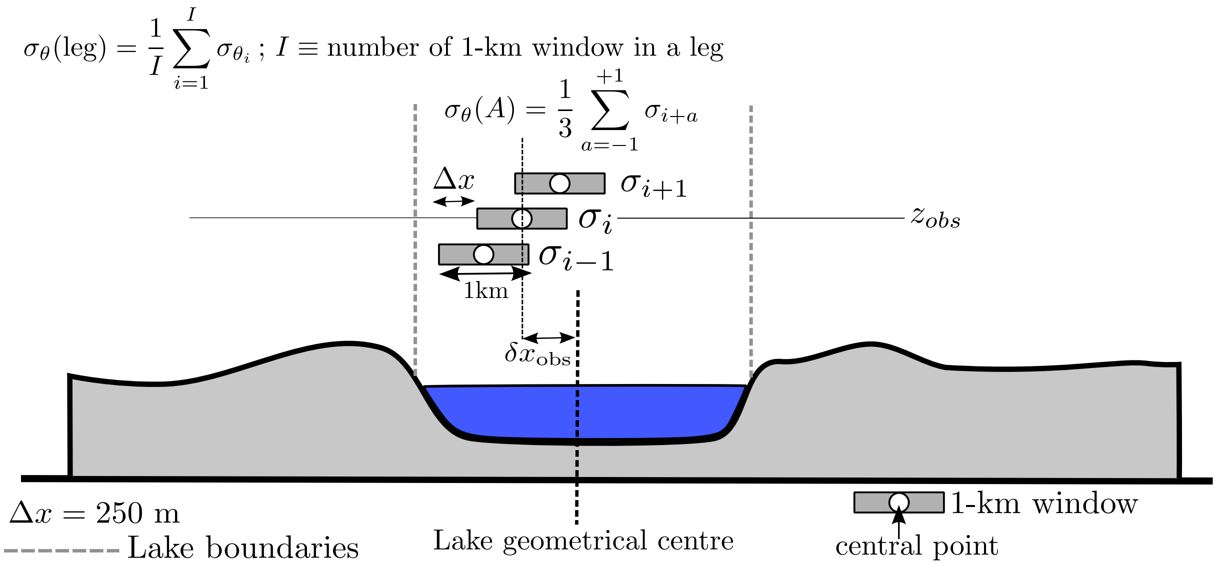

Figure 11: Schematics for the drop search σ_θ in the vicinity of the lake for three consecutive 1-km windows. Note that the sketch is not true to scale.

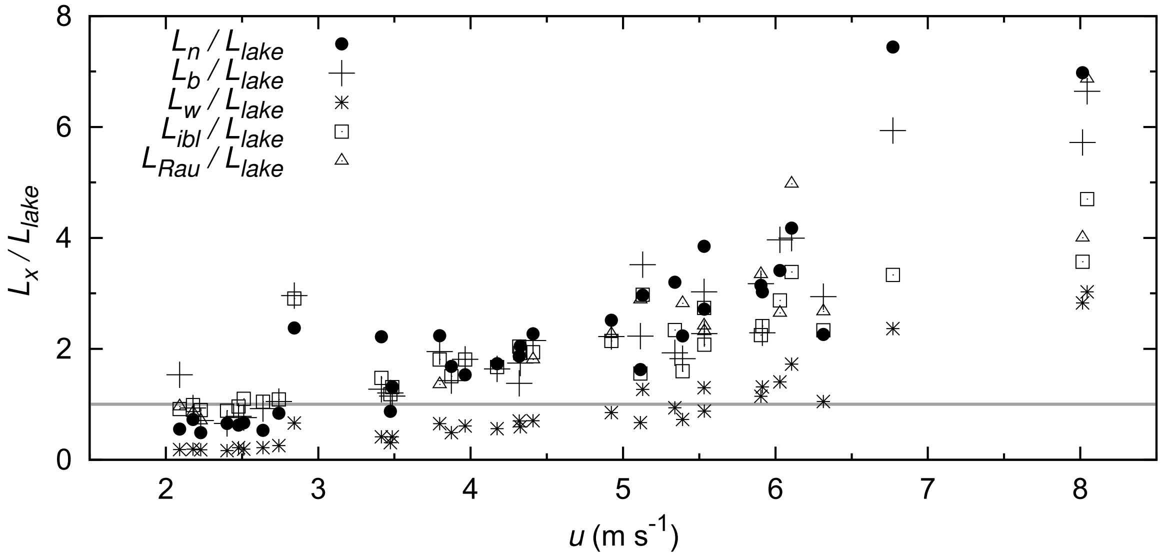

Figure 12: Estimation of the minimum horizontal length scale of the surface heterogeneity that is needed to influence the airborne measurements at the mean observation level for each leg as a function of the leg-averaged wind speed. The x-axis shows the ratio of the particular length scale and the actual geometrical length of the lake, which was crossed by each flight leg. The estimation of the length scale follows the blending-height parameterization for the near-neutral case ($L_{\mathrm{n}}/L_{\mathrm{lake}}$), the modified case after considering the surface heat flux ($L_{\mathrm{b}}/L_{\mathrm{lake}}$) and the generalized case ($L_{\mathrm{w}}/L_{\mathrm{lake}}$). Additionally, boundary-layer convective scaling has been calculated for those cases where the boundary-layer height was available ($L_{\mathrm{Rau}}/L_{\mathrm{lake}}$), and minimum length scale for detecting the formation of an IBL ($L_{\mathrm{ibl}}/L_{\mathrm{lake}}$). Horizontal straight gray line at $L_x/L_{\mathrm{lake}} = 1$ indicates where the geometrical length scale L_{lake} is equal to the minimum length scale L_x.

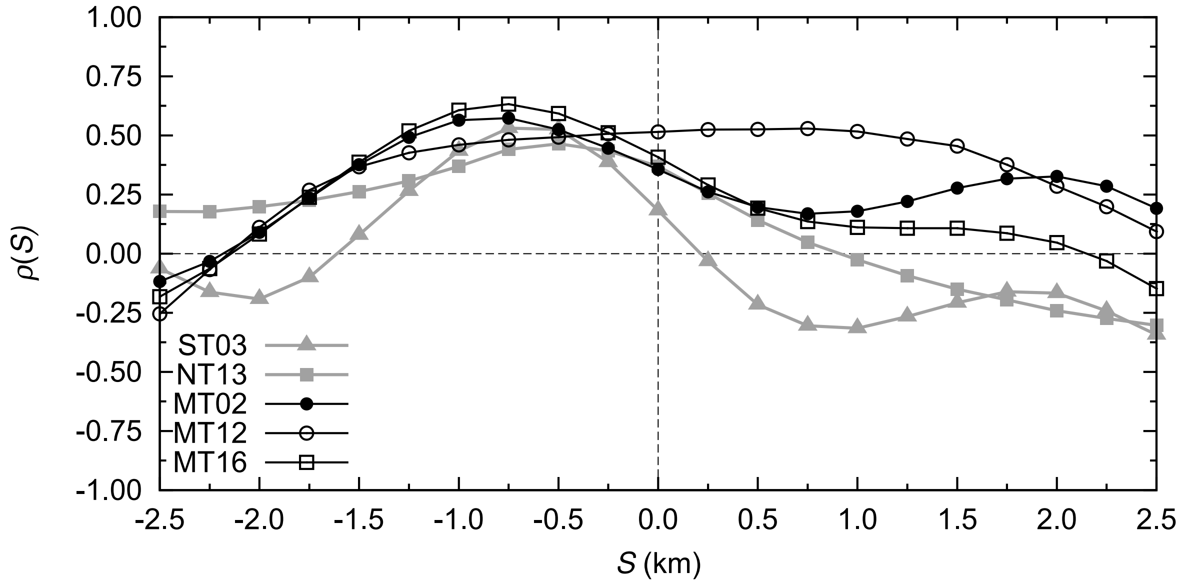

Figure 13: Cross-correlation function $\rho(S)$ between the standard deviation of potential temperature σ_θ and surface radiation temperature T_0 for the five legs of STI09 flight performed below 100 m.

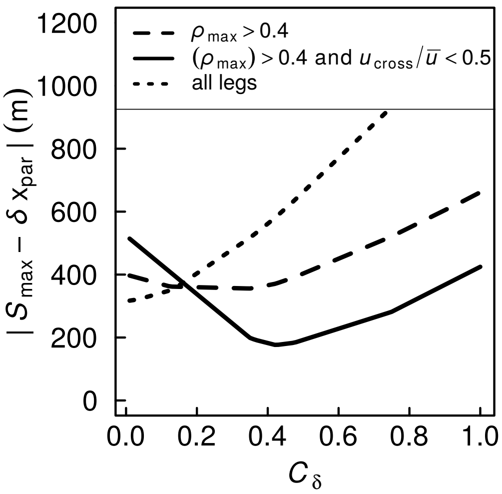

Figure 14: Absolute difference between the parameterized horizontal shift δx_{par} and the spatial lag of the maximum correlation function S_{max} against C_δ. For all legs (pointed line), legs with $\rho_{max} > 0.4$ (dashed line) and legs with $\rho_{max} > 0.4$ and low cross wind $u_{cross}/\overline{u} < 0.5$ (black line).

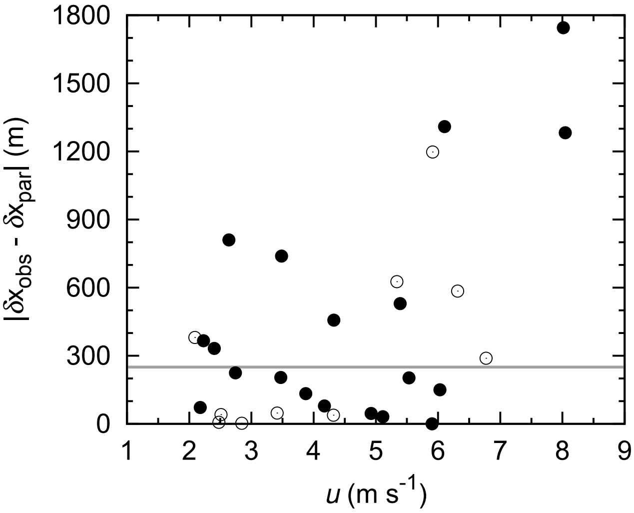

Figure 15: Absolute difference between the parameterized horizontal shift δx_{par} and the observed one δx_{obs} against the mean wind speed $\overline{u}$. A total of 29 legs with a clear drop of σ_θ in the vicinity of the lake could be observed. Open circles indicate those cases with $u_{cross}/\overline{u} > 0.5$ (large cross-leg winds). Black circle indicate cases with low cross wind $u_{cross}/\overline{u} < 0.5$. The horizontal grey line indicates the spatial lag between two consecutive overlapping windows (250 m).